Net irrigation requirement under different climate scenarios using AquaCrop over Europe

Louise Busschaert[1], Shannon de Roos[1], Wim Thiery[2], Dirk Raes[1], Gabriëlle J. M. De Lannoy[1]

[1]Department of Earth and Environmental Sciences, KU Leuven, Heverlee, B-3001, Belgium
[2]Department of Hydrology and Hydraulic Engineering, Vrije Universiteit Brussel, Brussels, B-1050, Belgium

Correspondence to: Louise Busschaert (louise.busschaert@kuleuven.be)

Abstract. Global soil water availability is challenged by the effects of climate change and a growing population. On average 70% of freshwater extraction is attributed to agriculture, and the demand is increasing. In this study, the effects of climate change on the evolution of the irrigation water requirement to sustain current crop productivity are assessed by using the FAO crop growth model AquaCrop version 6.1. The model is run at 0.5° lat x 0.5° lon resolution over the European mainland, assuming a general C3-type of crop, and forced by climate input data from the Inter-Sectoral Impact Model Intercomparison Project phase three (ISIMIP3).

First, the ~~performance of~~ AquaCrop surface soil moisture (SSM) ~~simulations using~~ forced with two types of ISIMIP3 historical meteorological ~~input from two ISIMIP3 forcing~~ datasets is evaluated with satellite-based SSM estimates in two ways. When driven by ISIMIP3a reanalysis meteorology ~~for the years 2011-2016~~, daily simulated SSM values have an unbiased root-mean-square difference of 0.08 and 0.06 m^3m^{-3} with SSM retrievals from the Soil Moisture Ocean Salinity (SMOS) and Soil Moisture Active Passive (SMAP) missions, respectively~~.~~, for the years 2015-2016 (2016 is the end year of the reanalysis data). When forced with ISIMIP3b meteorology from five Global Climate Models (GCM) for the years ~~2011~~2015-2020, the historical simulated SSM climatology closely agrees with the ~~climatology of the reanalysis-driven AquaCrop SSM climatology as well as the~~ satellite-based SSM climatologies.

Second, the evaluated AquaCrop model is run to quantify the future irrigation requirement, for an ensemble of five GCMs and three different emission scenarios. The simulated net irrigation requirement (I_{net}) of the three summer months for a near and far future climate period (2031-2060 and 2071-2100) is compared to the baseline period of 1985-2014, to assess changes in the mean and interannual variability of the irrigation demand. Averaged over the continent and the model ensemble, the far future I_{net} is expected to increase by ~~67~~22 mm ~~year~~month^{-1} (+30%) under a high emission scenario Shared Socioeconomic Pathway (SSP) 3-7.0. Central and southern Europe are the most impacted with larger I_{net} increases. The interannual variability of I_{net} is likely to increase in northern and central Europe, whereas the variability is expected to decrease in southern regions. Under a high mitigation scenario (SSP1-2.6), the increase in I_{net} will stabilize around ~~40~~13 mm ~~year~~month^{-1} towards the end of the century and interannual variability will still increase but to a smaller extent. The results emphasize a large uncertainty in the I_{net} projected by various GCMs.

1

1 Introduction

Global crop production has vastly increased over the past century, leading to the expansion of irrigated areas by almost sixfold, and more pressure on the irrigation water demand (Siebert et al., 2015). With changing climatic conditions and a growing population, future water availability is expected to further decline, raising demands for more efficient irrigation systems (Elliott et al., 2014; Taylor et al., 2013) and a higher crop water productivity (Brauman et al., 2021). In this context, a range of modelling studies have tried to assess future impacts on agricultural water demands and possible actions, but this remains a difficult task due to high uncertainties in future climate and socioeconomic scenarios (Elliott et al., 2014; Haddeland et al., 2014; Wada et al., 2013).

Future meteorological variables are typically modelled by Global Climate Models (GCMs) for different scenarios, usually represented by the Representative Concentration Pathways (RCPs; van Vuuren et al., 2011). Some challenges associated with climate forcing data are the consistency and the representation of the uncertainty of the data. The Inter-Sectoral Impact Model Intercomparison Project (ISIMIP) is an initiative to provide consistent bias-corrected climate datasets for impact modelling (Rosenzweig et al., 2017; Warszawski et al., 2014). The project is currently at its third simulation round (ISIMIP3) and provides reanalysis historical climate (ISIMIP3a) and GCM-driven historical and future climate (ISIMIP3b), following different emission scenarios, and using various GCMs. Data from the previous simulation round (ISIMIP2) have already been used in several studies of historical and future water resources (e.g. Boulange et al., 2021; Gudmundsson et al., 2021; Lange et al., 2020; Pokhrel et al., 2021; Reinecke et al., 2021).

Based on such climate projections, it is possible to derive meteorological drought indicators, which are determined by precipitation (P) and the atmospheric evaporation demand (ET_0). These meteorological droughts propagate into agricultural and hydrological droughts, characterized by a reduction in the soil water content and a reduction in streamflow. Over this century, droughts are expected to become more frequent in the northern hemisphere (Sheffield and Wood, 2008), in most parts of Europe (Spinoni et al., 2018, Grillakis, 2019), and especially in southern Europe (Pokhrel et al., 2021; Russo et al., 2013, Ruosteenoja et al., 2018). Common meteorological drought indices are directly associated to variations in P and ET_0 (Vicente-Serrano et al., 2015). The difference between these two fluxes ($P-ET_0$), also referred to as the climatic water balance, has served as proxy to investigate drying trends (Greve et al., 2014; Prăvălie et al., 2019). For agriculture, $P-ET_0$ is also a major factor determining the need for additional water, i.e. for irrigation.

In Europe, rainfall fulfills the largest part of the crop water requirement (green water), but irrigation (blue water) becomes essential in the most southern parts of the continent (Chiarelli et al., 2020; Liu and Yang, 2010; Siebert and Döll, 2010). For the past decades, the yearly net irrigation requirement in Europe has been estimated between 53 to 1120 mm year^{-1} in Denmark and Spain, respectively (Wriedt et al., 2009). The effectively applied amounts of irrigation could be much lower or higher but are unknown due to the lack of good observational data (Massari et al., 2021). Future global and regional irrigation trend assessments have commonly used hydrological models (e.g. WaterGAP [Döll and Siebert, 2002] in Döll, 2002; ~~Pfister~~Schadlach et al., ~~2011~~2012), agro-ecosystems models (Lund-Potsdam-Jena managed Land model [LPJmL, Bondeau et

2

al., 2007] in Fader et al., 2016; Konzmann et al., 2013), or agro-ecological zone (AEZ) models (FAO-AEZ methodology applied in Fischer et al., 2007). The earliest global study addressing future irrigation requirement under climate change was performed by Döll (2002) using the WaterGAP model for two GCMs. The results indicate clear effects on the long-term average irrigation requirement, with an average global increase of ~10% by the 2070s under the IPCC IS92a scenario (Leggett et al., 1992). Similar increases were found later by Fischer et al. (2007) also using two GCMs applied to an emission scenario from the IPCC Special Report on Emission Scenarios (SRES A2r; Nakicenovic et al., 2000; Riahi et al., 2007). By contrast, global decrease in irrigation water demand were simulated by Pfister et al. (2011) and Konzmann et al. (2013) for the end of the century. These studies only assessed one emission scenario, both from the IPCC SRES (Nakicenovic et al., 2000), namely the A1B and A2 scenario, respectively. However, in Europe, all these studies indicate clear increases in irrigation water requirement for most parts of the continent where irrigation is currently applied.

The outcomes of the different irrigation assessments can diverge quite significantly. Wada et al. (2013) provided an ensemble of seven General Hydrological Models (GHMs, including LPJmL and WaterGAP) and analyzed the sources of uncertainty on the final predictions. The results showed that the fraction of the variance due to the GCMs is larger than the fraction caused by the future emission scenarios, and that the largest partmore than 50% of the variance resulted from the GHMs, accounting for more than 50%.. The experiment setup also plays a major role as many parameters can influence the irrigation requirement. Global figures are highly different depending on whether the expansion of irrigated areas is considered or not, which explains why Fischer et al. (2007) found increases in the average water requirement, whereas Pfister et al. (2011) and Konzmann et al. (2013) expected a global decrease. The conclusions also depend on (i) whether irrigation efficiencies are considered (i.e., including socio-economic factors), (ii) the delineation of the growing season (a whole year, fixed or flexible start) and (iii) the type of implementation of irrigation in the model (gross or net requirement, threshold to trigger irrigation, amount of water applied; Telteu et al., 2021).

The irrigation requirement can also be estimated with crop models, which have the added benefit of estimating future trends in crop production and thereby provide useful information to farmers and decision-makers in their adaptation management strategies under climate change. Crop models mainly aim to present quantitative knowledge about the crop development and crop yield for a given crop having specific features and subject to given environmental conditions (Monteith, 1996). Crop modelling integrates physiological processes and the interactions between the crop and its environment. Several studies have shown the added value of upscaling field-scale crop models to a regional level (e.g. Balkovič et al., 2013; Boogaard et al., 2013; de Wit and van Diepen, 2007; Stöckle et al., 2014), allowing current and future crop yield and irrigation assessments. Liu and Yang (2010) used a GIS-based version of the EPIC (Williams et al., 1989) crop model to spatially evaluate the crop consumptive water use, partitioning the precipitation input, and the irrigation requirement for the year 2000. Pfister et al. (2011) used CROPWAT (Smith, 1992) to compute the global increase in irrigation requirement to meet future food and biomass demands. Elliot et al. (2014) provided estimations of futurethe potential irrigation water consumption with 10 GHMs (similarly to Wada et al., 2013) and six Global Gridded Crop Models (GGCMs developed within the Agricultural and Model Intercomparison Project (AgMIP) framework, Rosenzweig et al., 2014), of which three are upscaled site-based crop models.

3

Global-scale crop modelling remains challenging, especially at coarser resolutions (e.g. 0.5° x 0.5° lat-lon), where one grid cell may contain information of many heterogeneous agricultural fields (Müller et al., 2017). In addition, field management practices (e.g. irrigation practices, fertilizer application) are even more challenging to integrate at regional and global levels. In this study, the spatial version of AquaCrop developed by de Roos et al. (2021) will be used. AquaCrop (Steduto et al, 2009; Raes et al., 2009) set up as a field-scale model, was developed by the Food and Agriculture Organization of the United Nations (FAO) and is based on the soil water balance. Compared to other, more complex canopy-level models, AquaCrop stands out by its relatively few and intuitive input parameters (Steduto et al., 2009). AquaCrop has already been used in regional agricultural climate impact studies by Dale et al. (2017), where an open-source version of AquaCrop (AquaCrop-OS; Foster et al., 2017) was used to project crop yields for a high number of GCMs under different climate scenarios at a resolution of 2°- x 2°.

In this study, the impact of climate change on the future net irrigation requirement is assessed for different emission scenarios and GCMs, using the spatial version of AquaCrop (de Roos et al., 2021) forced with ISIMIP3 meteorological data over the European continent for the first time. First, the model performance is evaluated by comparing historical spatial AquaCrop v6.1 simulations without any irrigation, ~~and~~ forced with (i) reanalysis ~~and~~data from ISIMIP3a and (ii) GCM-based meteorological data from ~~ISIMIP3a and~~ ISIMIP3b, against satellite-based surface soil moisture (SSM) observations. Next, AquaCrop v6.1 simulations are performed using an ensemble of five ISIMIP3b GCMs as forcing to provide estimates of changes in the net irrigation water requirement (I_{net}) during the summer months (June, July, August) for two periods in the future (2031-2060 and 2071-2100). The focus is mainly on estimating water demand during the summer period and not on crop water productivity. The objective is to regionally quantify the mean and interannual variability in summer I_{net} for a near and future climate period, and relate this to the current (baseline) I_{net} and future changes in P-ET_0 following various climate scenarios. Compared to previous studies, the advantages are that the simulations are performed with (i) climate data from the latest generation of reanalyses and GCMs, (ii) the most recent set of future scenarios, and (iii) a crop model (AquaCrop), in which the dynamic interactions between water and vegetation are the main focus and where irrigation and management practices can be included with more detail than in a land surface or hydrological model. Future I_{net} projections could be used to inform on climate change adaptation strategies (e.g., climate-smart irrigation, crop type selection, water conservation). The new AquaCrop-ISIMIP3 model setup can be run at any spatial domain and resolution, providing future opportunities for further climate analysis, also including other irrigation practices and management options.

2 Model and data

2.1 Model setup

The study domain includes the European continent, with latitudes (lat) ranging from 34.75° N to 59.75° N, and longitudes (lon) from -10.75° E to 41.25° E. The spatial and temporal resolutions of the model simulations are set to those of the ISIMIP3 input datasets, i.e. 0.5° lat x 0.5° lon, and daily time steps. The same spatial AquaCrop (v6.1) model structure as described by

4

de Roos et al. (2021) is used for this study, but adaptations are made to the spatial resolution, input datasets, and simulated periods. Simulations are performed from 1985 through 2100, either with or without considering irrigation, and with the respective associated crop-related parameters.

2.2 Model parameters

Climate impact assessments are subject to large uncertainties, which increase with longer temporal projections. Therefore, several assumptions are made in this study to limit the uncertainty of other factors than climate. We will present net irrigation requirement values that are independent of the irrigated area, period, infrastructure and the exact crop type. First, simulations are performed over all pixels of the entire study domain (i.e. the main European continent), and the irrigation estimates for the entire hypothetically irrigated agricultural domain are normalized by area to make the results independent of the actual irrigated area. This avoids the need to include estimates of future hypothetical land use (Prestele at al., 2016), and the uncertain evolution of the extent of irrigated areas (Schaldach et al., 2012; Hurtt et al., 2020). Second, the spatial resolution of this study matches that of the ISIMIP input data resolution. In contrast to fine-scale agricultural studies, usually assessing actual irrigation under historical conditions, future climate projections are dependent on the resolution of the driving climate models (or downscaled output). Such studies mainly aim at estimating the irrigation requirement that is needed for crop root uptake, thereby omitting the part of irrigation that is lost to the atmosphere, or retained on the soil surface or in the soil profile. Also, state-of-the-art global and continental-scale climate impact assessments are typically performed at the same resolution (e.g., Jägermeyr et al., 2021; Lange et al., 2020; Thiery et al., 2021). Third, each pixel is defined as a hypothetical homogeneous field, in which the vegetation conditions are identical. For future projections, the use of a representative field crop is supported by the current lack of detailed year- and location-specific crop maps, and by the unpredictability of changes and developments in crop type and distribution. Finally, the uncertainty and high spatial and temporal variability of the start and end of the growing season (King et al., 2018; Menzel and Fabian, 1999; Schadlach et al., 2012) restricts the modelling possibilities. Some previous studies (e.g., Elliott et al., 2014; Fader et al., 2016; Fischer et al., 2007; Konzmann et al., 2012) have used dynamic growing seasons, but the choice has been made to avoid this additional level of uncertainty for this study. Therefore, only the summer months are considered to make the future requirement directly comparable to the baseline I_{net}. On average, these are the months presenting the highest I_{net} (Siebert and Döll, 2010), and are expected to remain important months for irrigation requirements, even if growing seasons might shift in the future.

Soil data is extracted from the ISIMIP3 soil input dataset that has been used in the AgMIP GGCM intercomparison (GGCMI; Rosenzweig et al., 2014). ISIMIP3 uses the Harmonized World Soil Database version 1.2 (HWSD1.2), aggregated to 0.5° resolution. The soil dataset represents dominant soil types on croplands within each pixel. Two soil layers are implemented in AquaCrop: one topsoil layer of 0.30 m, and an underlying layer of 1 m, both with the same ISIMIP (topsoil only) textural properties (clay, sand, silt fractions) and gravel content, but with different derived soil hydraulic parameters. More specifically, the volumetric soil water content at saturation, field capacity, and permanent wilting point (θ_s, θ_{FC}, θ_{PWP}) and the saturated hydraulic conductivity (K_{sat}) are derived using depth-specific (topsoil, subsoil) pedotransfer functions described by De Lannoy

et al. (2014). Because the crop rooting depth is set to 1 m and various bedrock maps indicate that the soil depth over Europe reaches below 1 m (Dirmeyer and Oki., 2002; Mahanama et al., 2015; Shangguan et al., 2017), no limitations to root development in a 1 m soil depth need to be considered (Raes et al., 2009). A total profile depth of 1.30 m is defined, but without the presence of a groundwater table or confining layers, the actual depth below the maximum rooting depth has no influence on the simulations.

To assessFor the irrigation water requirement over timehistorical model evaluation with satellite retrievals, the choice is made to use a general C3-type of crop with a 1-m rooting depth to describe the vegetation component, similar to de Roos et al. (2021). This choice is motivated by the coarse spatial resolution and the high uncertainty in crop modifications over time and follows the methodology of well-known hydrological and land surface models, that also make use of general vegetation descriptions (e.g. Niu et al., 2011; Rodell et al., 2004).

For the historical model evaluation with satellite retrievalsC3 crops are dominant in Europe (Monfreda et al., 2008; Still et al., 2003). A detailed description of the crop characteristics is given in Table 1 of de Roos et al. (2021). For the model evaluation, no irrigation is activated, the soil fertility stress of 30% is maintained (de Roos et al., 2021), and the AquaCrop default record of mean annual CO_2 concentration observed at Mauna Loa (Hawaii, USA) is considered in the simulations. By contrast, the simulations with irrigation follow the yearly CO_2 concentrations of the emission scenarios from ISIMIP3 and assume near-optimal soil fertility.

For the determination of I_{net}, a representative field crop is considered. The crop characteristics that determine crop transpiration and hence I_{net} are listed in Table 1. The considered crop transpiration coefficient of 1.10 is a good indicative value of the basal crop coefficient for the mid-season for a large range of field crops (Allen et al., 1998). Moreover, it is assumed that in the summer months (in which I_{net} is determined) the crop has reached its maximum canopy cover and is prior to senescence. Since I_{net} is determined by keeping the soil water content in the root zone above 50 % of the readily available water (RAW, which is 25 % of the total available water, TAW, for the representative field crop), water stress does not affect crop transpiration. Also, air temperature stress affecting crop transpiration will be small or absent in the summer months with the settings of the thresholds in Table 1. To be sure of a well-developed crop canopy during the three summer months, it is assumed in the simulations with irrigation, that the crop germinated in early spring, and that the natural crop senescence occurred in late autumn. Irrigated fields are assumed to be well-managed. Hence, a near-optimal soil fertility is defined in AquaCrop, corresponding to a potential achievable biomass production (without any other stress) of 80% (compared to 70% for the simulations without irrigation). To be sure of a well-developed crop canopy during the three summer months, it is assumed in the simulations with irrigation, that the crop germinated in early spring, and that the natural crop senescence occurred in late autumn. Future elevated CO_2 concentrations are expected to increase biomass production by reducing crop transpiration and stimulating crop production (CO_2 fertilization effect; Vanuytrecht et al., 2012). This response can vary according to intrinsic crop characteristics or nutrient availability (Vanuytrecht et al., 2011). To avoid overexpression of this effect, the sink term in AquaCrop is lowered to 0%.

Table 1. Characteristics of the representative field crop

Crop parameters	values	units
Canopy cover (during the 3 summer months)	85	% soil cover
Crop transpiration coefficient when canopy is complete	1.10	-
Maximum effective rooting depth	1.0	m
Soil water depletion at which stomata starts to close	50	%TAW
Base temperature, below which crop development does not progress	8.0	°C
Minimum growing degrees required for full crop transpiration	10.0	°C-day

2.3 Meteorological data

The AquaCrop model is run with both reanalysis (ISMIP3a) and GCM-based (ISIMIP3b) meteorological input. The ISIMIP3a
200 forcing data extend up to end 2016 and are based on bias-corrected ECMWF Reanalysis data fifth generation (ERA5; Cucchi
et al., 2020; Lange, 2019a). The GCM (ISIMIP3b) data start in 2015 and are derived from five different GCMs contributing
to the Coupled Model Intercomparison Project phase 6 (CMIP6): GFDL-ESM4, IPSL-CM6A-LR, MPI-ESM1-2-HR, MRI-
ESM2-0, UKESM1-0-LL (Lange, 2019b, 2020). These future climate data are separated into different scenarios, which are
based on the new scenario framework described by van Vuuren et al. (2014), combining RCPs (van Vuuren et al., 2011) with
205 pathways of socioeconomic development (shared socioeconomic pathways SSPs; O'Neill et al., 2014). The sixth assessment
report of the IPCC (2021) demonstrates its results based on this scenario architecture. Scenarios are referred to as SSP*x-y*,
where SSP*x* refers to the SSP (five in total, described in O'Neill et al., 2014), and *y* refers to the level of radiative forcing (in
W m^{-2}) in 2100 (RCP). ~~Under SSP3-7.0 and SSP5-8.5, global warming of 2 °C will likely be exceeded by mid-century.~~ Three
scenarios are evaluated, SSP1-2.6 (low emissions thanks to strong mitigation), SSP3-7.0 (high emissions), and SSP5-8.5
210 (extreme emissions or unmitigated), for five GCMs, resulting in a total of 15 SSP-GCM scenarios. Under SSP3-7.0 and SSP5-
8.5, a global warming of 2 °C will likely be exceeded by mid-century.

AquaCrop requires minimum and maximum temperature, rainfall, and reference evapotranspiration (ET$_0$), on a daily basis.
Meteorological variables extracted from ISIMIP3 are the daily maximum and minimum temperatures, total precipitation, near-
surface relative humidity, near-surface wind speed (at a 10 m height), and the shortwave downwelling radiation. Daily ET$_0$
215 values are estimated with the FAO Penman-Monteith equation according to the guidelines presented in the FAO Irrigation and
Drainage Paper 56 (Allen et al., 1998) with the available variables and ISIMIP elevation data (for the estimation of the
atmospheric pressure).

2.4 Satellite-based evaluation data

To evaluate the performance of the regional AquaCrop simulations forced with ISIMIP input, two L-band microwave-based

220 level 2 SSM products are used: (i) the SMUDP2 data product version 650 from the ESA Soil Moisture Ocean Salinity (SMOS) mission (Kerr et al., 2010), from 2011 onwards; and (ii) the SPL2SMP product version 7 from the NASA Soil Moisture Active Passive (SMAP) mission (Chan et al., 2016), from 2015 onwards. For both data sources, only recommended quality retrievals are included. Additionally, retrievals for daily minimum temperatures below 4 °C are screened out to avoid retrievals near frozen conditions. Both satellite products are projected on a 36-km Equal-Area Scalable Earth version 2 (EASEv2) grid, for

225 SMOS data after reprojection as in De Lannoy and Reichle (2016). It should be noted that SMOS data over Europe have been affected by radio frequency interference and are filtered out, especially in the early years after launch in 2010 (Oliva et al., 2012).

3 Methodology

3.1 Simulations

230 Three types of ~~simulations (~~simulation experiments~~)~~ are performed and referred to as SIM1, SIM2, and SIM3, ~~represented~~with the corresponding settings described in ~~the scheme in Fig. 1.~~Table 2. SIM1 and SIM2 constitute the historical model evaluation~~.~~ against satellite retrieval products. For ~~the first simulation (~~SIM1~~),~~, reanalysis meteorological data (ISIMIP3a) are used as input and simulated SSM is compared to satellite reference data~~. The earliest SMOS SSM observations are available in 2011.~~ ~~Therefore,~~ at a daily resolution (short-term variability). AquaCrop is run over the study area for the period from 1 January

235 2011 through 31 December 2016 with reanalysis data, i.e. until the end of the available reanalysis data. The second set of historical simulations (SIM2) are ~~historical~~ GCM-driven (ISIMIP3b) SSM simulations. The purpose of SIM2 is to determine whether the GCM-based forcing is reliable to use for future simulations~~.~~, i.e. via an evaluation of multi-year average SSM (long-term distribution). For each GCM, AquaCrop is run with climate input data for the period 2011-2020. These input data gather historical simulated climate for 2011-2014, and scenario-based simulated climate for the period 2015-2020, only

240 accounting for SSP5-8.5 (only small differences occur between the three SSPs for this time period). The meteorological time series of the two periods are stitched together to provide continuous AquaCrop forcing fields for 2011-2020. SIM1 and SIM2 have a spin up period of four years, and only output from 2015 onwards is used for evaluation, i.e. starting when both SMOS and SMAP data are available.

Once the model has been evaluated with the first two experiments, simulations of SIM3 are run with GCM-driven

245 meteorological input (ISIMIP3b) for the baseline (historical reference period, 1985-2014) and into the future from 2021 through 2100. ~~The~~Irrigation is activated in AquaCrop and the net irrigation water requirement I_{net} for the three summer months is extracted from ~~these~~the simulations for the reference time window, and two future time horizons (near future 2031-2060, and far future 2071-2100). For the baseline simulation, the initial moisture conditions are set to field capacity while the future

8

periods have a spin up of at least 10 years (continuous simulation from 2021 through 2100). For SIM3, ~~AquaCrop~~irrigation is
250 ~~run with~~introduced, using the net irrigation requirement option in AquaCrop, whereby a small amount of water (just covering
the crop ET for that day) is injected into the root system on days when a certain fraction of the ~~Readily Available soil Water~~
~~(~~RAW~~)~~ is depleted (Raes et al., 2017). With this option, solely the amount water taken up by the roots is considered, where
the wetting of the soil surface, and interval and application amount specific to a particular irrigation method are not relevant.
By selecting a threshold of 50~~-~~% RAW depletion, which is the average depletion in an optimal irrigation interval (Smith, 1992),
255 crop water stress affecting the canopy development and transpiration of the ~~generic C3~~representative field crop is avoided, and
effective rainfall (the part stored in the root system up to field capacity) is still considered. All simulations performed in this
research are uncoupled, i.e. feedback mechanisms from irrigation on atmospheric climate (e.g. Hirsch et al., 2017; Thiery et
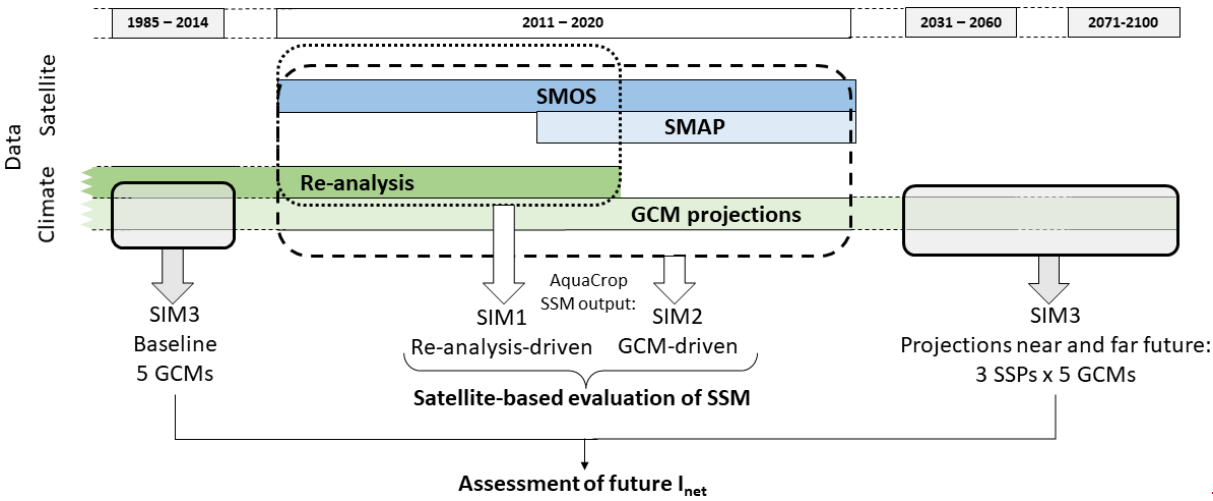al., 2017, 2020) are neglected.

260

~~Figure 1 Schematic presenting~~

Table 2 Description of the different simulations ~~of this study,~~ with ~~an overview of satellite and~~ regard to the simulation periods, analyses,
climate data ~~availability. Note that the SIM3 baseline period (1985-2014) was separated from~~, crop characteristics, soil fertility stress and
the ~~from~~ activation of the ~~present-day period (2011-2020) for readability purpose.~~irrigation (ON/OFF).

265

Sim.	Period	Analysis	Climate data	Crop	Soil fertility stress (%)	Irrigation
SIM1	April 2015 - December 2016	SSM short-term evaluation	reanalysis	generic C3	30	OFF
SIM2	April 2015 - December 2020	SSM climatological evaluation	5 GCMs	generic C3	30	OFF

SIM3	1985-2014	I_{net} projections	5 GCMs	representative	20	ON
	2031-2060		5 GCMs x 3 SSPs	field crop		
	2071-2100					

3.2 Evaluation of historical AquaCrop simulations

3.1.1 Skill metrics

To compare the spatial and temporal patterns of SSM from 0.5° AquaCrop simulations with 36-km satellite data, nearest-neighbour sampling is used to spatially match simulated SSM with SMOS and SMAP retrievals. The output variable extracted
270 from the AquaCrop simulation is the volumetric water content of the topsoil compartment, corresponding to the first 0.1 m of the soil (output variable WC01 in AquaCrop). After quality screening of the satellite data (see section 2.4), about ~~1.4~~0.9 and 1.9 million usable observations are kept over the study domain (composed of 3882 pixels) for SMOS and SMAP, within the period ~~January 2011 – December 2020 and~~ April 2015 – December 2020~~, respectively~~. The most widely used validation metrics for SSM estimates from large-scale model simulations and retrievals are the Pearson correlation coefficient (R), the bias, the
275 root-mean-square difference (RMSD), and the unbiased RMSD (ubRMSD), which are calculated as follows:

$$R = \frac{\sum_{n=1}^{N}(x_n - \bar{x})(y_n - \bar{y})}{\sqrt{\left(\sum_{n=1}^{N}(x_n - \bar{x})^2\right)\left(\sum_{n=1}^{N}(y_n - \bar{y})^2\right)}} \tag{1}$$

$$bias = \frac{1}{N}\sum_{n=1}^{N}(x_n - y_n) \tag{2}$$

$$RMSD = \sqrt{\frac{1}{N}\sum_{n=1}^{N}(x_n - y_n)^2} \tag{3}$$

$$ubRMSD = \sqrt{RMSD^2 - bias^2} \tag{4}$$

280 where x are the simulated SSM, y the reference observations, N the number of observation-simulation pairs, and ($\bar{\ }$) is the temporal mean. A minimum threshold of N=100 reference data points in time are set per pixel for all analyses. ~~Because of the strong seasonal variation (wet winters and drier summers) of a temperate climate that characterises most of Europe, SSM correlations tend to be high and could misrepresent the validity of the model (Albergel et al., 2013). To avoid this effect, time series of anomalies are calculated by subtracting the climatology from the data for each daily time step. The climatology~~
285 ~~calculates the mean seasonal cycle as a long-term mean using a sliding window of 31 days with a minimum threshold of three data points of data within the window. Then, the Pearson correlation coefficient is calculated based on the anomaly time series (anomR).~~
Anomaly correlations are discussed in Appendix A.

3.1.2 Difference in evaluation ~~timescale~~ for SIM1 and SIM2

290 ~~The~~Both the time series of historical SIM1 and SIM2 SSM ~~(2011 through 2016)~~ are compared to satellite observations ~~(SMOS: 2011-2016, and SMAP: 2015-2016)~~ through the skill metrics described in section 3.1.1 for the time period with available data

10

for both SMOS and SMAP, i.e. from April 2015 through 2016. SIM1 is a short-term evaluation since daily SSM simulations are compared to satellite observations. All months of the year with available and qualitative satellite data were included in this first validation step.

295 For the historical SIM2 SSM simulations ~~(2011 through 2020),~~ the multi-year average (long-term) results driven by the five different GCMs ~~are also evaluated with SMOS (2011-2020),~~ and ~~SMAP (2015-2020) satellite observations. Additionally,~~ the median SSM time series across the GCMs ~~is~~are evaluated. However, for each simulation year, only the period between the 1st of March up to the 31st of October is considered ~~in the evaluation~~, because only summer months will be considered for the subsequent analysis of future I_{net} (section 3.2). Climate models are developed to indicate changing climatic trends but do not

300 present daily accurate data, if they are not constrained by observational data. Therefore, the multi-year average (i.e. climatology) of SIM2 SSM is computed ~~for the corresponding observation period for the five GCM driven simulations and their median. These can~~and then be compared to the climatologies of satellite ~~and reanalysis driven SSM~~SSM during the observation period, using the same skill metrics presented in section 3.1.1. Climatologies are calculated using a sliding window of 31 days with a minimum threshold of three data points of data within the window. The computation of the climatology is

305 restrained to the availability of reference satellite data (i.e. SMAP, data available from April 2015), as it is also the case in satellite data assimilation systems (e.g., SMAP Level 4 product; Reichle et al., 2019).

3.2 Future net irrigation I_{net} requirement (SIM3)

This study focuses on the evaluation of the change in I_{net} during the period for which the highest irrigation demand is expected in all parts of Europe, i.e. June, July, and August~~.~~ (Siebert and Döll, 2010). For the evaluation of the future irrigation water

310 requirement, daily I_{net} values (directly available from the model output) are first extracted from the SIM3 output of the 15 different SSP-GCM combinations~~, and~~. The results are ~~then summed for~~expressed in mm month^{-1} by averaging the I_{net} of the three summer months ~~for each simulated year. Although this is expressed in mm year^{-1}, it is important to stress that only the three summer months are considered~~. The summer irrigation is then used for evaluation following two approaches. First, the summer I_{net} is averaged over the 30-year time window allowing to compare future (2031-2060 and 2071-2100) and baseline

315 (1985-2014) average I_{net} by computing the difference (ΔI_{net}). A statistical t-test is carried out to define whether the difference of mean I_{net} between the two periods is significant ($p < 0.05$). Second, interannual variation is assessed based on the I_{net} range (RI_{net}), defined as the difference between maximum and minimum summer I_{net} of the 30-year time window. Again the difference between future and baseline RI_{net} is evaluated (ΔRI_{net}). I_{net} simulated for the different SSP-GCM combinations are analyzed individually. Additionally, the median results across the GCMs for each scenario are presented. A simple climate

320 index ($P-ET_0$), computed for the three summer months, is used to identify where drying trends are potentially occurring, and how this is reflected in the irrigation requirement.

4 Results

4.1 Evaluation of historical regional AquaCrop simulations forced with ISIMIP3

4.1.1 ~~SIM1: reanalysis-driven simulations~~ Short-term evaluation (SIM1)

325 AquaCrop SSM simulations forced with ISIMIP3a reanalysis data ~~for the years 2011-2016 (SIM1)~~ are evaluated ~~against~~with SMOS and SMAP SSM retrievals. ~~Only the SMOS SSM retrievals cover this entire reanalysis period, allowing to evaluate the short-term and interannual variability in the AquaCrop SSM in terms of temporal anomR. Figure 2 shows the anomR over Europe with a spatial mean anomR of 0.44. Higher correlations are found in south-western locations (anomR often > 0.6) and lower performances occur in north and central-western Europe (anomR generally < 0.4). Also shown on this figure is a~~
330 ~~partitioning of Europe in various zones for further discussion.~~
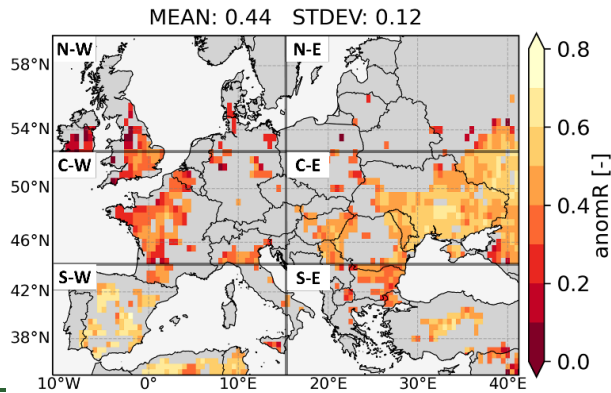
~~**Figure 2** Anomaly correlation (anomR) between SIM1 AquaCrop SSM and SMOS SSM for the period 2011-2016. The spatial mean and standard deviation are indicated (MEAN, STDEV). The six European sub-regions used to describe the model evaluation and the future I_net are indicated (from top left to bottom right: north-west, north-east, central-west, central-east, south-west, south-east).~~

335 ~~From~~ from April 2015 through December 2016~~,~~ (start when data from both ~~SMOS and SMAP SSM retrievals~~missions are available~~.~~, until end of reanalysis data). The spatially averaged skill metrics for AquaCrop SSM compared to satellite observations from SMOS and SMAP are presented in Table ~~1~~3. The skill is generally better relative to SMAP SSM than relative to SMOS SSM. The expected errors of both missions are 0.04 m^3m^{-3} when comparing the satellite data to in situ reference data (Entekhabi et al., 2014). Here, slightly higher ubRMSDs of 0.06 and 0.08 m^3m^{-3} are obtained.

340 **Table ~~1~~3** Spatial mean (± spatial standard deviation) of R, RMSD, bias, and ubRMSD between SIM1 SSM estimates, SMOS, and SMAP, for April 2015 through December 2016.

| Reference obs.	R (-)	RMSD (m^3m^{-3})	bias (m^3m^{-3})	ubRMSD (m^3m^{-3})
SMOS	0.53 (±0.13)	0.10 (±0.03)	-0.05 (±0.05)	0.08 (±0.02)
SMAP	0.65 (±0.15)	0.08 (±0.04)	-0.03 (±0.06)	0.06 (±0.01)
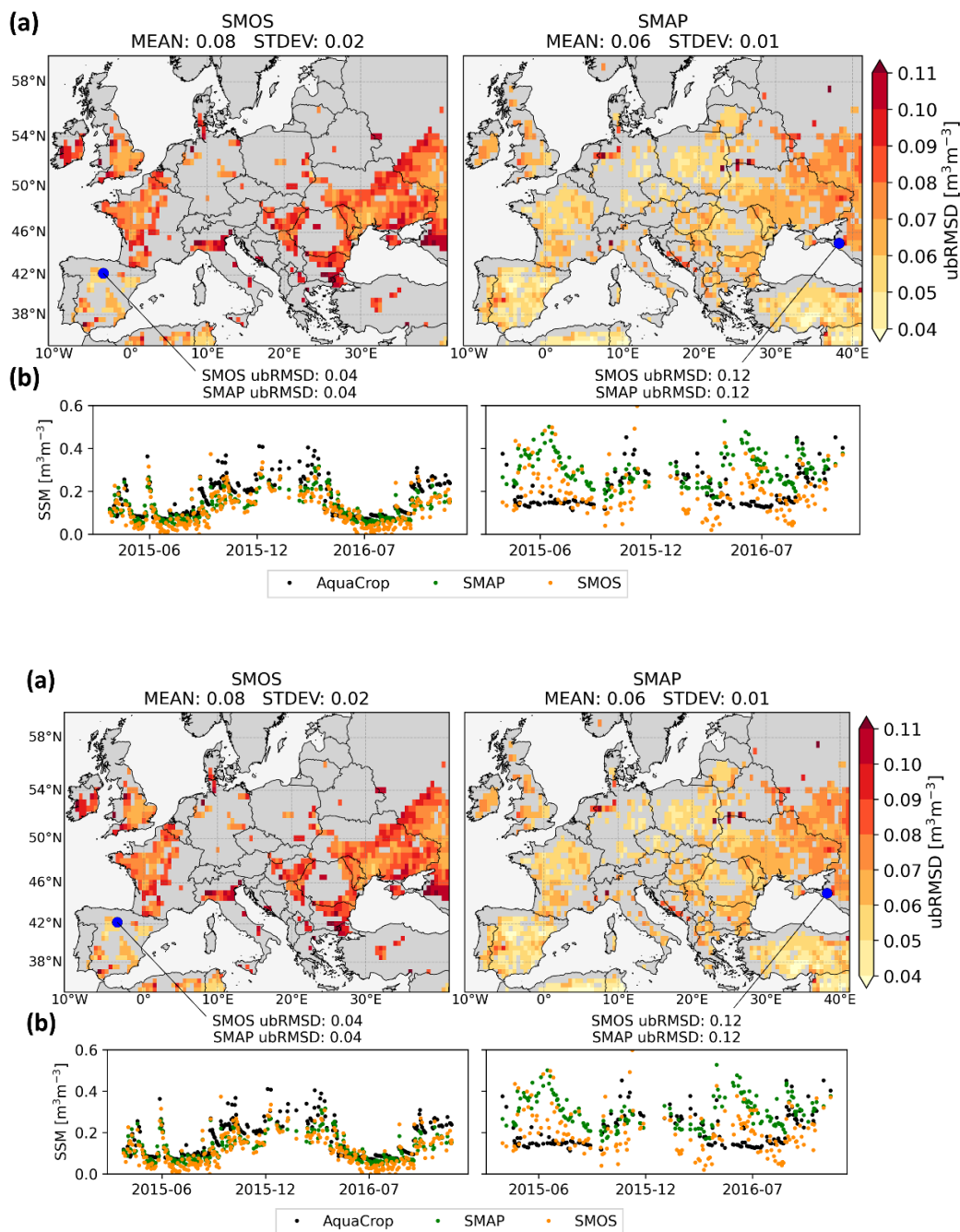
Figure ~~3~~1 (a) ubRMSD of SIM1 AquaCrop SSM compared to SMOS (left) and SMAP (right) retrievals for April 2015 through December 2016. The spatial mean and standard deviation are indicated in the titles (MEAN, STDEV). (b) SSM time series of two pixels (marked by blue dots in (a) with the title indicating the ubRMSD [m³m⁻³] against SMOS and SMAP for each location.

The spatial distribution of ubRMSD is presented in Fig. ~~3a.~~1a. For further discussion, a partitioning of the study domain in various shown is presented in Appendix A (Fig. 1A). Simulated SSM deviate more from SMOS retrievals in north and central-

eastern Europe, whereas pixels located in southern regions (e.g. Spain) present a better model performance when comparing to SMOS. Central-eastern Europe presents on average a higher ubRMSD, stressing a lower performance in this region. Time series of SSM estimates at two locations are shown in Fig. ~~3b~~1b. The ~~modeled~~modelled SSM contents are close to satellite retrievals for the first pixel (left), and a mismatch is found between simulations and retrievals for the second pixel (right). For the latter, AquaCrop simulations are underestimating SSM during summer and it can be noticed that SMOS and SMAP retrievals substantially diverge for this location.

### 4.1.2 Climatological evaluation (SIM2~~: GCM-driven simulations~~)

The SIM2 AquaCrop SSM for the period 2011-2020 is forced with ISIMIP3b GCM-driven meteorology. The ~~10 years of daily~~ modelled SSM ~~are~~is converted to a multi-year average climatology for the five GCMs, and compared to climatologies of SMOS ~~(2011-2020)~~ and SMAP SSM (2015-2020) ~~SSM, as well as SIM1 SSM (2011-2016),~~ for the months March through October. Spatially averaged temporal skill metrics are shown in Fig. ~~4. The climatologies are inevitably computed for different numbers of samples in time~~2.
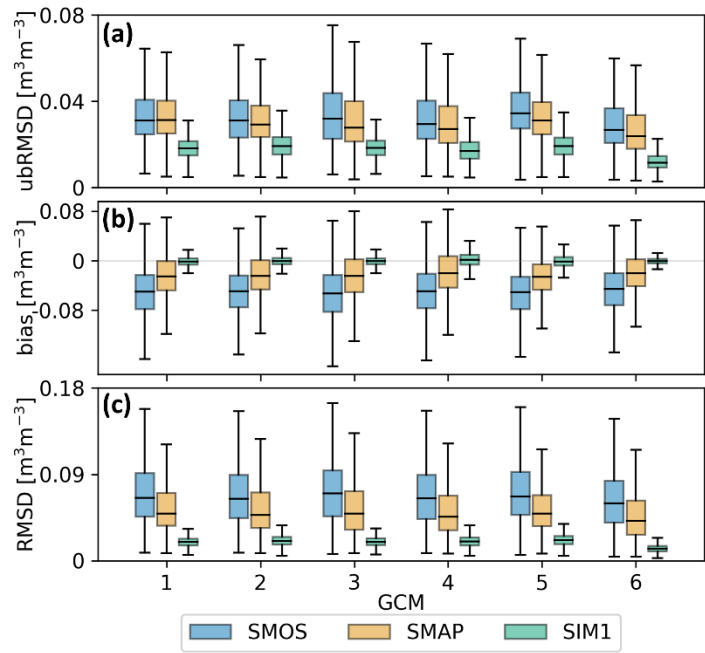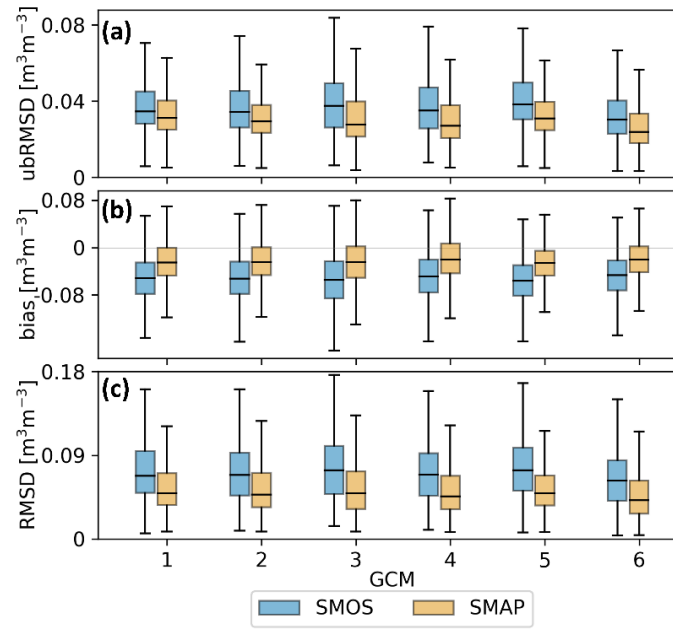
Figure 42 Spatial boxplots of (a) ubRMSD, (b) bias, and (c) RMSD, for five GCMs (1 to 5: GFDL-ESM4, IPSL-CM6A-LR, MPI-ESM1-2-HR, MRI-ESM2-0, UKESM1-0-LL) and the median across GCMs (6). SIM2 SSM is compared with ~~(i)~~ SMOS ~~SSM for 2011-2020~~ (blue, left~~), (ii))~~ and SMAP (yellow-brown, right) SSM for April 2015 through December 2020 ~~(yellow-brown, middle), and (iii) SIM1 SSM for 2011 till 2016 (green, right)~~. Only SSM values for the months March through October are considered in the computation of the skill metrics, and the spatial coverage is different for ~~each boxplot (full coverage for SIM1 only).~~ SMOS and SMAP. The boxes represent the values in the interquartile range (IQR), the line in the box corresponds to the median, and the whiskers extend to Q1 – 1.5IQR and Q3 + 1.5IQR, or are cut off if all data points fall into the interval (outliers are not shown).

All GCM-driven simulations are similarly biased compared to the satellite products. The larger dry bias with SMOS (on average -0.05 m³m⁻³) compared to SMAP observations (on average -0.02 m³m⁻³) agrees with the <u>short-term</u> evaluation results of the reanalysis-driven simulations (section 4.1.1). ~~The bias of SSM climatologies between the GCM-driven to reanalysis-driven simulations, is minimal (green boxplots in Fig. 4b), indicating that GCM-driven projections are representative of the reanalysis climate. Moreover, the~~ The evaluation of predicted SSM compared to satellite data results in spatially averaged mean ubRMSDs ranging between 0.02 and 0.04 m³m⁻³, with the lowest values for the multi-model median SSM (Fig. ~~4a~~2a).


15
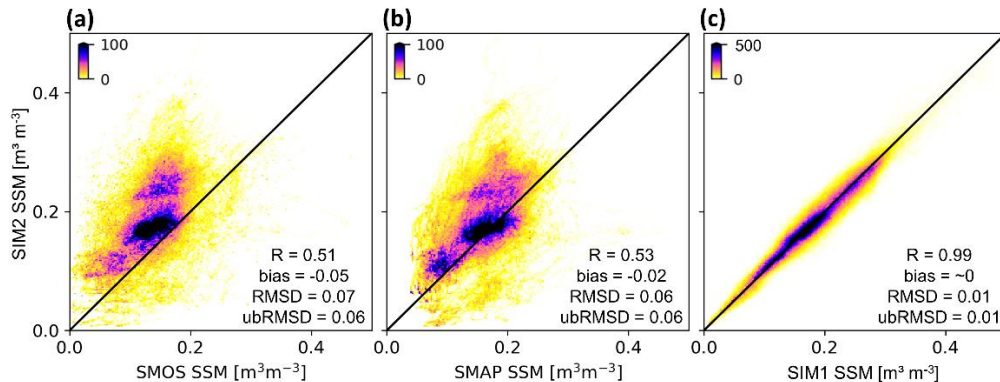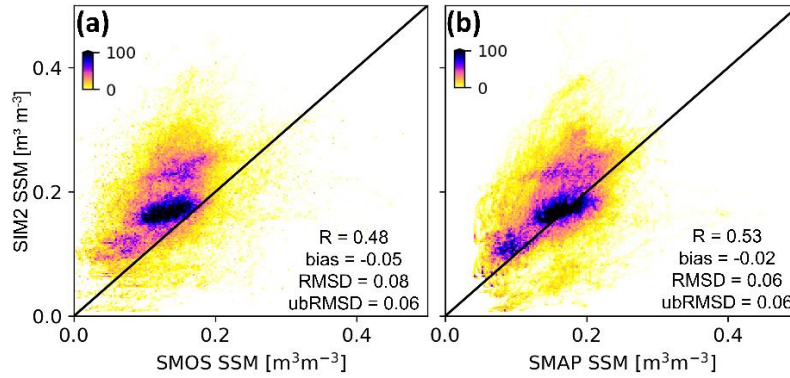
Figure ~~5~~3 Density scatter plots comparing the SIM2 SSM climatology (median climatology across the GCMs), against a reference climatology based on (a) SMOS retrievals ~~(2011-2020),~~ (b) SMAP retrievals (April 2015-2020~~), and (c) SIM1 SSM estimates (2011-2016)~~). Only the period from 1 March to 31 October is considered. The colorbars represent the number of space-time samples per bin. Spatio-temporal skill metrics (R, bias, RMSD and ubRMSD) are shown.

Figure ~~5~~3 presents the spatio-temporal skill metrics comparing the multi-model median SIM2 SSM climatology with ~~three referencethe~~ the two satellite-based SSM climatologies. The GCM-driven SSM climatology remains close to satellite SSM climatologies in drier conditions but there is a wet model bias (or dry satellite retrieval bias) in wetter conditions (Fig. ~~5a and b). By contrast, no spatio-temporal pattern bias is seen between GCM-driven and reanalysis-driven SSM climatologies (Fig. 5c), i.e. SIM1 and SIM2 simulations are well correlated in all moisture conditions (R=0.99).~~3). Correlations between simulated climatologies and satellite data are slightly lower when considering individual GCMs (no median) with ranges of 0.~~46~~41-0.~~49~~45 and 0.47-0.51 for SMOS and SMAP, respectively (not shown). By design, GCM climatolgies are unbiased against the reanalysis climatology, indicating that GCM-driven projections are representative of the reanalysis climate. From the evaluation of SIM1 and SIM2, it can overall be concluded that AquaCrop forced by ISIMIP3 input demonstrates a reasonable performance in terms of spatio-temporal SSM pattern representation; we therefore assume that the model can be used to project I_{net} changes across the study area.

## 4.2 Future net irrigation requirement I_{net} (SIM3)

4.2.1 Climate impact on mean I_{net}

The change in summer I_{net} is assessed by the difference (ΔI_{net}) between the mean I_{net} of the future horizons (2031-2060; 2071-2100) and the baseline period (1985-2014). In Fig. ~~6~~4, spatial boxplots of ΔI_{net} are presented for five GCMs individually and for the median across the GCMs for each scenario.

16
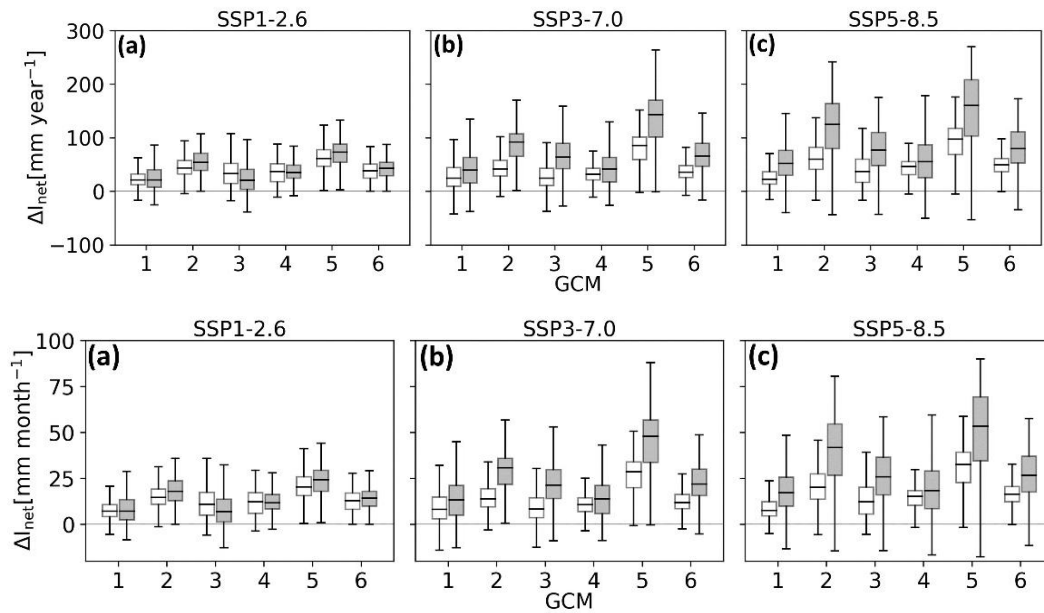
Figure 6̶4 Spatial boxplots of ΔI_{net} [mm ~~year~~month^{-1}] for the three SSPs (a, b, c) and five GCMs (1 to 5: GFDL-ESM4, IPSL-CM6A-LR, MPI-ESM1-2-HR, MRI-ESM2-0, UKESM1-0-LL) and the median across GCMs (6), for near (2031-2060: white) and far (2071-2100: grey) future, both relative to the baseline period (1985-2014).

Based on Fig. 6̶4, increases in I_{net} are expected in the future for all scenarios, where the severity of the increase depends on the emission scenario. SSP1-2.6 presents a stabilization of I_{net} towards the end of the century in line with the evolution of CO_2 for this scenario, whereas the other scenarios show increases from 2031-2060 to 2071-2100. The differences between the GCMs within an SSP are considerable and these disparities increase with rising emission ~~scenario~~scenarios. According to the first GCM (GFDL-ESM4), on average about 2̶07 mm ~~year~~month^{-1} extra irrigation water will be required in the summer months by 2050 for SSP5-8.5, whereas for UKESM1-0-LL, ~~nearly 100~~more than 20 mm ~~year~~month^{-1} will be required by mid-century for the same emission scenario. Decreases in I_{net} (boxplot whiskers below 0, Fig. 4c) are only observed in a few southern coastal locations~~, especially along the Mediterranean coast and~~ under the ~~highest~~high and severe emission ~~scenario (Fig. 6c).~~scenarios. In these historically warm and dry regions with insignificant rainfall in the summer months, the effect of stomatal closure by 5% as response to CO_2 concentrations above 550 ppm is stronger than the increase in ET (less than 5%). These negative differences are ~~mostly~~ statistically non-significant (except for GFDL-ESM4, but the total area subjected to decreases is negligible). Figure 7̶5 presents the spatial distribution of ΔI_{net}, for the median across the GCMs. Regions where all GCMs present significant changes are stippled. Once the results are presented in terms of medians, ~~virtually~~ no statistically significant decrease in ΔI_{net} is observed.
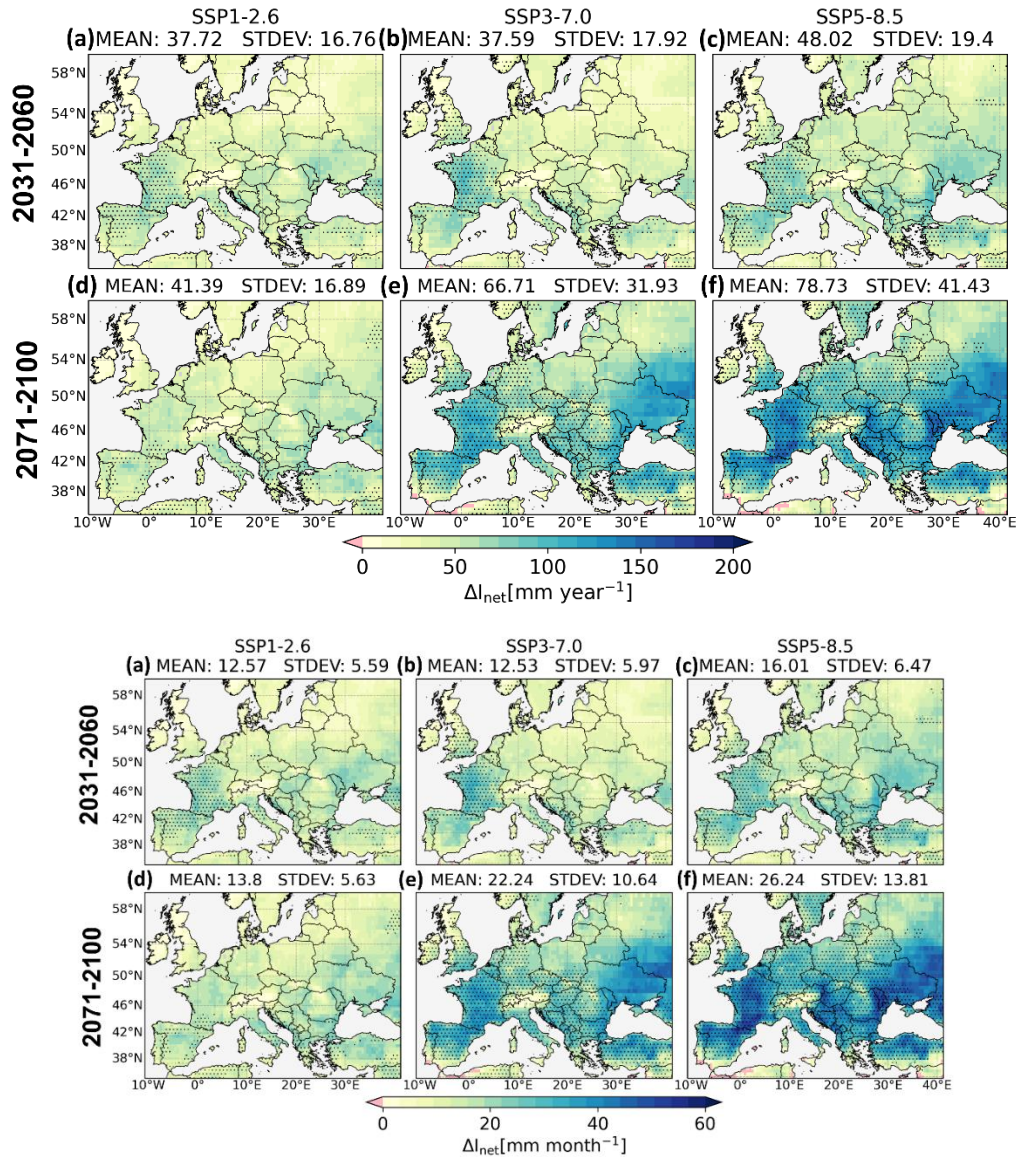
Figure 75 Changes in summer I_{net} (ΔI_{net}~~),~~) [mm month^{-1}], median across five GCMs for the two future time horizons (rows) and the three scenarios (columns) with reference to the baseline period. The stippled areas represent pixels where all five GCMs present statistically significant changes (t-test, $p < 0.05$).

Under the low emission scenario (Fig. ~~7a~~5a and d), the whole continent will face a mild increase in summer I_{net} by about ~~40~~ 13 mm ~~year~~ month^{-1} (+18%) in the near and far future, and regions undergoing severe increases cannot be identified. Towards the end of the century, for high and extreme emissions, the most affected areas (where all GCMs agree on a significant change) are situated in the central and southern latitudes (Fig. ~~7e~~5e and f). For the end of the century, the spatial mean summer I_{net} increases by ~~67~~22 and ~~79~~26 mm ~~year~~month^{-1} (+30% and +35%) for SSP3-7.0 and SSP5-8.5, respectively. The most eastern parts are on average presenting large ΔI_{net} for the far future (2071-2100), but according to GFDL-ESM4 alone (not shown),

18

these changes are non-significant and therefore not stippled in Fig. ~~7e~~5e and f. All SSP-GCM combinations agree on the evolution of I_{net} in the northern Alps, where the situation is likely to remain stable, in terms of amounts of required irrigation water.
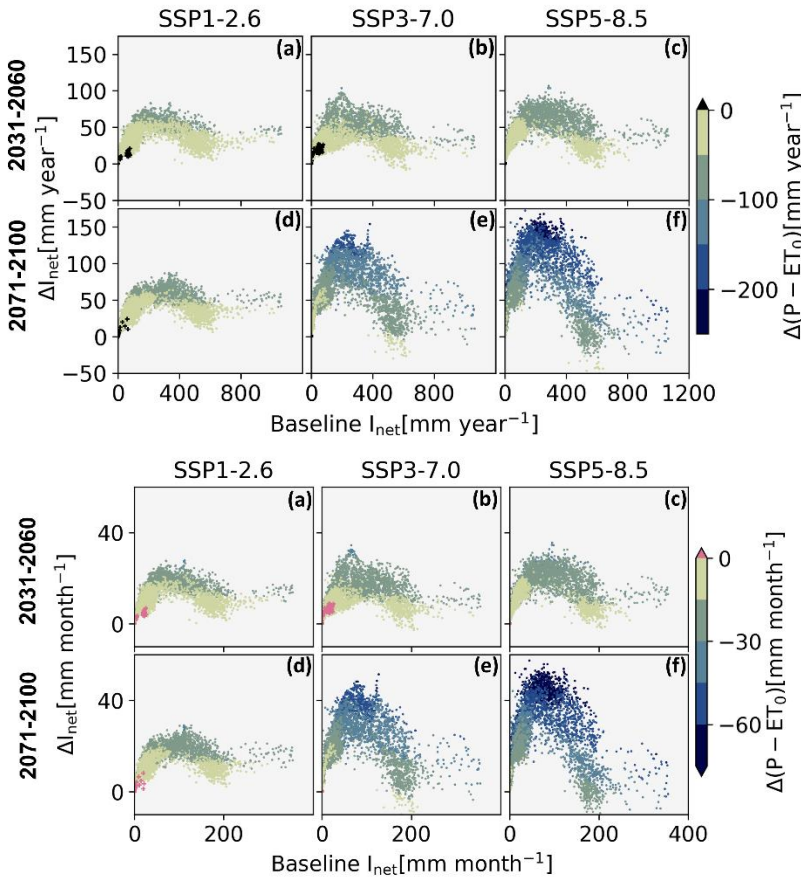
Figure ~~8~~6 Scatter plots of ΔI_{net} relative to the baseline period for the two future periods (rows) and the three scenarios (columns). The coloring refers to the corresponding $\Delta(P\text{-}ET_0)$. Increases in ~~$\Delta(P - ET_0)$~~$\Delta(P\text{-}ET_0)$ are represented by ~~black~~pink crosses. All values (I_{net} and ~~$\Delta(P - ET_0)$~~$\Delta(P\text{-}ET_0)$) are medians across the GCMs~~.~~ [mm month^{-1}].

Figure ~~8~~6 shows the spatial relationship between the expected change in summer I_{net} with reference to the baseline period. Areas with historically extreme (> ~~500~~150 mm month^{-1}) or low (< ~~100~~20 mm month^{-1}) I_{net} will not see their future needs increase drastically, whereas regions with a relatively moderate to high baseline I_{net} will face the strongest changes. Table ~~2~~4 summarizes the baseline summer I_{net} and ΔI_{net} (median and standard deviation across GCMs), for six selected countries and the Benelux included in this study area. The difference between the ΔI_{net} for various scenarios is of the same order of magnitude as, and often smaller than, the variability introduced by the various GCMs. Note again that the presented numbers are expressed in mm ~~year~~month^{-1}, but only ~~integrated~~averaged over three summer months ~~per year~~, and the results are purely based on climate projections that are integrated into AquaCrop, assuming a hypothetical C3 crop, near-optimal fertilization, and without accounting for the presence or quality of the irrigation network.

19

Table ~~2~~4 Median across GCMs (± standard deviation of GCMs) of baseline summer I_{net}, ~~ΔI_{net},~~ ΔI_{net}, baseline RI_{net}, and ~~ΔRI_{net}~~ (ΔRI_{net} [mm ~~year~~month^{-1}~~)~~], spatially averaged over the country, for six European countries and the Benelux. The changes ~~Δ~~Δ are presented for the two future horizons (2031-2060 and 2071-2100, columns), and for the different emission scenarios (line 1, 2, 3 of a cell corresponding to SSP1-2.6, SSP3-7.0, and SSP5-8.5, respectively).

	Summer I_{net} (mm ~~year~~month^{-1})			RI_{net} (mm ~~year~~month^{-1})		
Country	**Baseline**	**Δ 2031-2060**	**Δ 2071-2100**	**Baseline**	**Δ 2031-2060**	**Δ 2071-2100**
Benelux	~~77 (±7~~26 (±2)	~~37 (±13)~~	~~43 (±26)~~	~~198 (±43~~66	~~38 (±21)~~	~~25 (±34)~~
		~~42 (±24)~~	~~71 (±42)~~	(±14)	~~43 (±49)~~	~~106 (±33)~~
		~~53 (±19~~12	~~94 (±39~~14		~~36 (±32~~13	~~63 (±34~~8
		(±4)	(±9)		(±7)	(±11)
		14 (±8)	24 (±14)		14 (±16)	35 (±11)
		18 (±6)	31 (±13)		9 (±3)	21 (±11)
France	~~159 (±65~~3	~~56 (±15)~~	~~50 (±19)~~	~~261 (±29~~87	~~19 (±26)~~	-~~3~~ (±8)
	(±2)	~~66 (±17)~~	~~94 (±42)~~	(±10)	~~10 (±36)~~	10 (±~~25~~13)
		~~73 (±28~~19	~~121 (±37~~17		~~36 (±38~~6 (±9)	~~29 (±38)~~
		(±5)	(±6)		3 (±12)	19 (±~~69~~6
		22 (±6)	31 (±14)		12 (±13)	(±23)
		24 (±9)	40 (±12)			
Germany	~~80 (±5~~27 (±2)	~~32 (±17)~~	~~40 (±30)~~	~~189 (±44~~63	~~24 (±25)~~	~~3 (±36)~~
		~~39 (±26)~~	~~59 (±55)~~	(±15)	~~28 (±28)~~	~~81 (±40)~~
		~~43 (±30~~11	~~82 (±56~~13		~~57 (±32~~8 (±8)	~~63 (±48~~1
		(±6)	(±10)		9 (±9)	(±12)
		13 (±9)	20 (±18)		19 (±11)	27 (±13)
		14 (±10)	27 (±19)			21 (±16)
Italy	~~275 (±59~~2	~~39 (± 8)~~	~~46 (±10)~~	~~231 (±24~~77	-~~15 (±37~~5	-~~35 (±34)~~
	(±2)	~~38 (±10)~~	55 (±~~15~~ (±3)	(±8)	(±12)	-~~15 (±32)~~
		~~39 (±18~~13	18 (±7)		9 (±26)	-~~12~~ (±11~~ (±31)~~
		(±3)	22)		3 (±~~27~~9)	-5 (±11)
		13 (±3)	~~66 (±22~~ (±7)		1 (±9)	-4 (±10)
		13 (±6)				
Romania	~~153 (±75~~1	49 (±23)	43 (±22)	~~242 (±50~~81	7 (±14)	~~61 (±26)~~
	(±2)	~~36 (±32)~~	~~85 (±49)~~	(±17)	14 (±21)	~~23 (±33)~~
		~~56 (±29~~16	~~109 (±42~~14		20 (±41)	~~55 (±47~~20
		(±8)	(±7)		42 (±62)	(±9)

21

	12 (±11)	28 (±16)		60 (±3110)	8 (±11)	
	19 (±10)	36 (±14)			18 (±16)	
Spain	412 (±3137	48 (±12)	40 (±16)	259 (±1686	-12 (±154 (±5)	-17 (±326
	(±1)	51 (±24)	71 (±13 (±5)	(±5)	-10 (±233 (±8)	(±11)
		56 (±2216	24 (±11)		-1 (±250 (±8)	-36 (±3112
		(±4)	28)			(±10)
		17 (±8)	85 (±23 (±8)			-26 (±149 (±5)
		19 (±7)				
Ukraine	197 (±866	60 (±20 (±7)	59 (±23)	300 (±31100	-11 (±434	26 (±27)
	(±3)	40 (±32)	112 (±50)	(±10)	(±14)	23 (±42)
		61 (±3113	122 (±5020		-27 (±439	1 (±329 (±9)
		(±11)	(±8)		(±14)	8 (±14)
		20 (±10)	37 (±17)		41 (±3714	0 (±11)
			41 (±17)		(±12)	

Figure 86 also shows how the atmospheric conditions in the summer, i.e. $\Delta(P-ET_0)$, are directly related to ΔI_{net}. The largest increases in ΔI_{net} correlate with strong decreases in $P-ET_0$. The few locations showing a positive $\Delta(P-ET_0)$ in SSP1 2.6 (black crosses in Fig. 8a6a, b and d) are still subjected to a slight increase in irrigation requirement. The ΔI_{net} estimates obtained with AquaCrop provide additional information over the mere $\Delta(P-ET_0)$ estimates, because the soil-plant system has a memory and temporally integrates the past $P-ET_0$ and irrigation events. Since the crop and management parameters are constant for the entire study domain, the only factor affecting I_{net} for a given climate (P and ET_0) is the buffering capacity of the root zone, i.e. soil characteristics. An analysis of the influence of soil characteristics showed, for instance, that sandy soils see their I_{net} enlarge more rapidly compared to loamy soils. However, no clear conclusions could be drawn, because the vast majority of Europe at the resolution of this study is dominated by a loamy soil texture.

### 4.2.2 Climate impact on the interannual variability of I_{net} (RI_{net})

To assess the potential change in interannual variability of summer I_{net}, the difference between the maximum and minimum summer I_{net} within a 30-year time period (range of I_{net} = RI_{net}) is evaluated. The future RI_{net} values are assessed with reference to the baseline period, resulting in ΔRI_{net} for each scenario and GCM. Results are presented in Fig. 97, where expansions of RI_{net} are indicated in red, and reductions in blue.
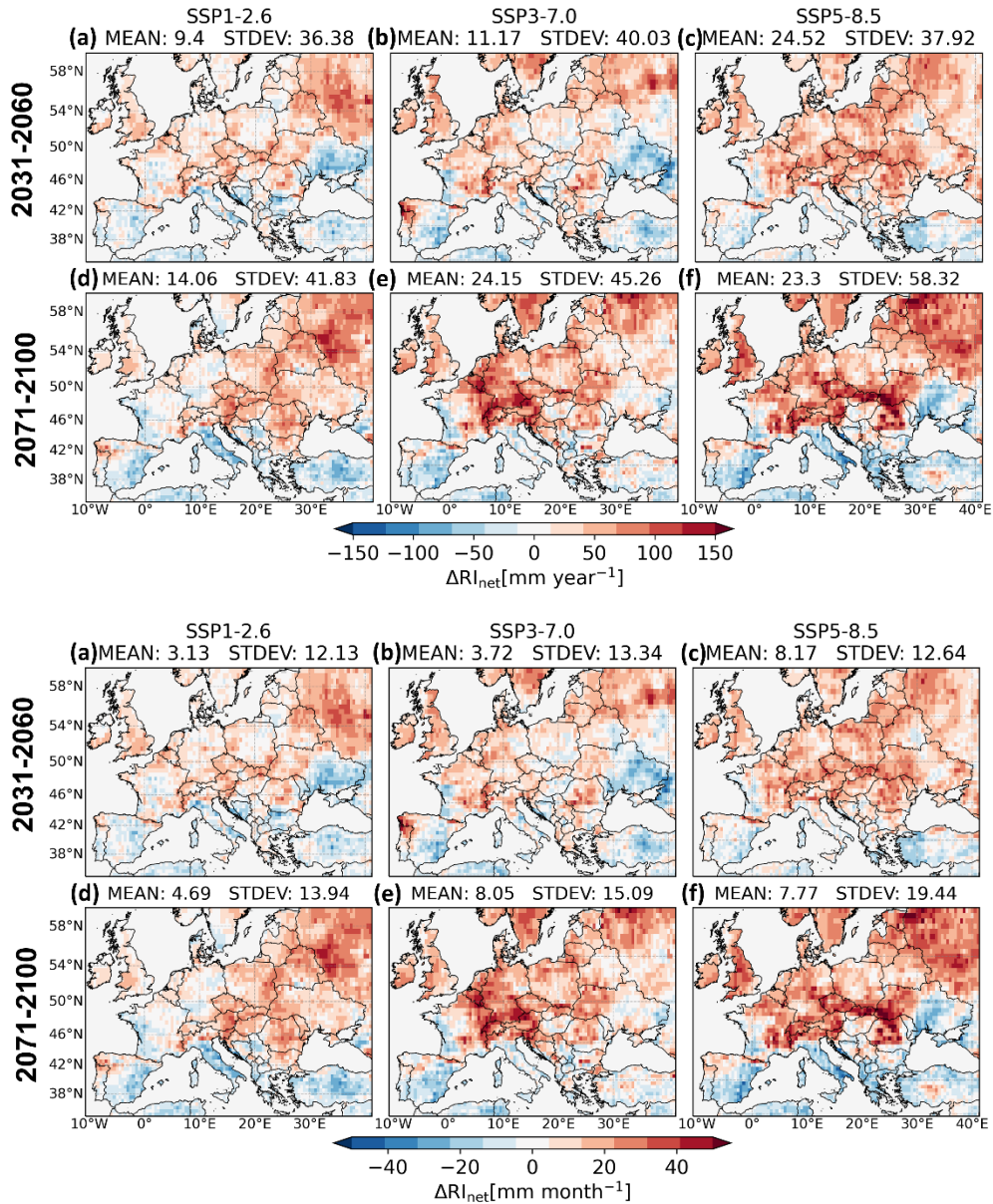
Figure 97 Future changes in RI_net (~~ΔRI_net~~ΔRI_net) [mm month^{-1}] median of five GCMs for the two future horizons (rows) and the three scenarios (columns) with reference to the baseline period.

470   For all SSPs, future RI_{net} are likely to decrease in most of southern Europe, whereas the gap between the highest and lowest irrigation requirement in the 30-year time window is expected to grow in northern and central regions of Europe. Similar to ΔI_{net} (Fig. ~~7~~5), Fig. ~~9~~7 shows that changes are strengthened from SSP3-7.0 to SSP5-8.5 (far future, Fig. ~~9e~~7e and f), in line with the expected increase in extreme events with climate change. Table ~~2~~4 summarizes the baseline RI_{net} and changes in interannual variability for some selected countries in Europe.
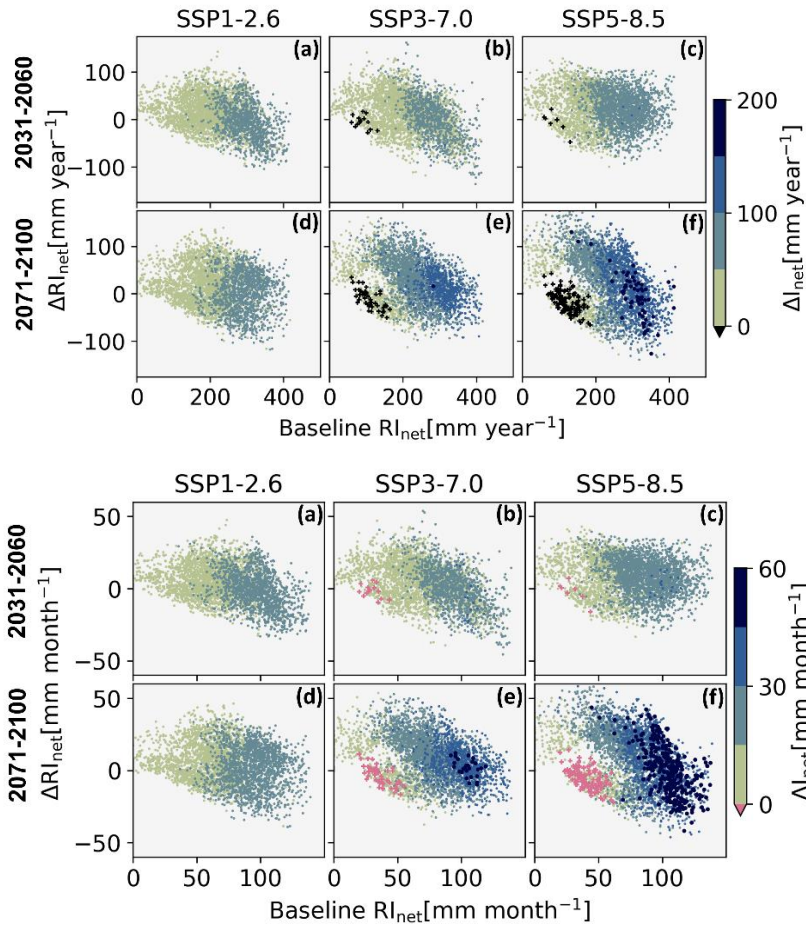
Figure ~~10~~8 Scatter plots of ~~ΔRI_net~~ΔRI_{net} versus baseline range for the two future periods (rows) and the three scenarios (columns). The dots are colored by ~~ΔI_net~~ΔI_{net} of the corresponding time window and scenario. Negative ~~ΔI_net~~ΔI_{net} are marked with ~~black~~pink crosses and extreme increases in ~~ΔI_net~~ΔI_{net} (> 45 mm ~~year~~month^{-1}) are represented as dark blue larger dots. All values (RI_{net} and ~~ΔI_net~~ΔI_{net}) are medians across the GCMs~~.~~ [mm month^{-1}].

Figure ~~10~~8 presents how the change in interannual variability (ΔRI_{net}) of the two future periods relates to the baseline RI_{net}, and to ΔI_{net}. Regions with severe increases in I_{net} do not necessarily present the highest enlargements in RI_{net}. The largest baseline RI_{net} correlate to lower ΔRI_{net} for the far future (SSP3-7.0 and SSP5-8.5, Fig. ~~10e~~8e and f), in combination with high values of ΔI_{net} (dark blue dots, Fig. ~~10e~~8e and f). In other words, the Mediterranean region, west France and the region around Black Sea, with currently a high interannual variability in irrigation requirements will see their requirement significantly increase to more steady high irrigation requirement. Large ΔRI_{net} values follow the Carpathian Mountains (central Europe) for SSP5-8.5 (Fig. ~~9f~~ 7f). According to the model, only little irrigation was required in these mountainous regions during the baseline whereas future requirement are projected to increase. In the future, I_{net} peaks to larger values for several years, increasing RI_{net}.
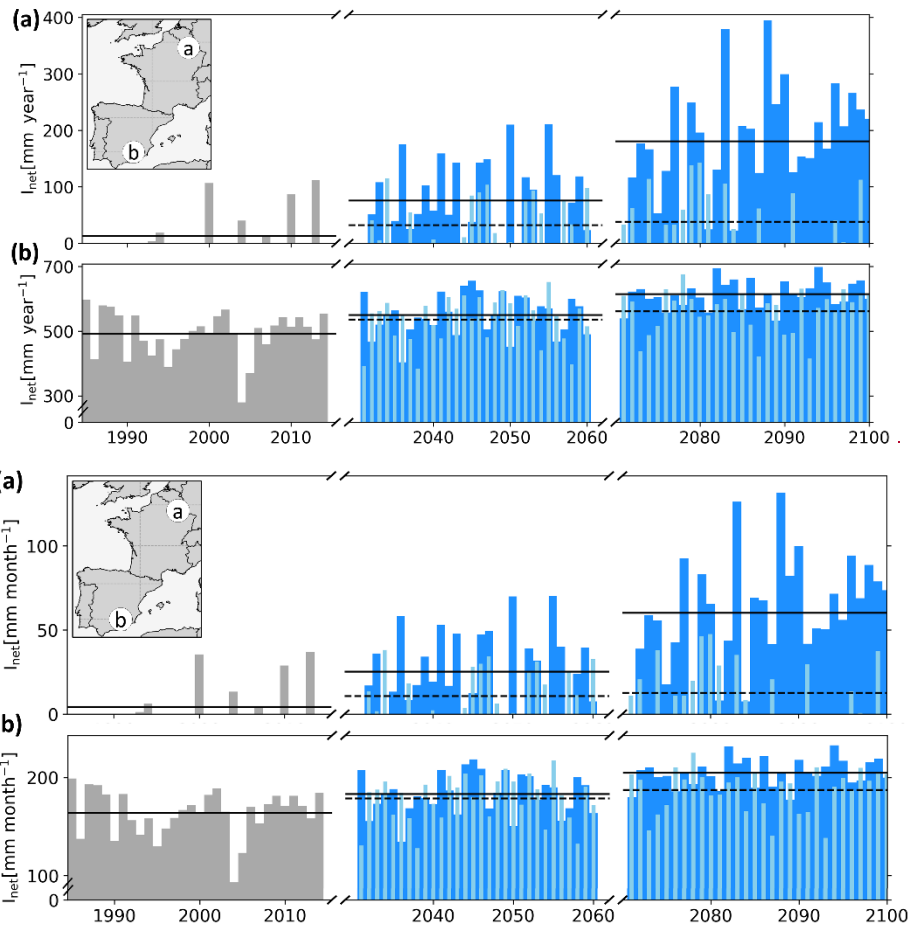
Figure ~~11~~2 Time series of summer I_{net} [mm month^{-1}] simulated with climate data extracted from IPSL-CM6A-LR for two locations (a) 49.75° N 5.25° E, and (b) 38.25° N 2.75° W, marked on the inset. SSP1-2.6 is represented by thin light blue bars, SSP5-8.5 by dark blue wider bars. The horizontal lines correspond to the time series mean over the climate window, for the future horizons the dotted lines correspond to SSP1-2.6 and the full lines to SSP5-8.5.

To get a better understanding of changes in interannual variability of I_{net}, time series ~~of~~at two different locations for one GCM are presented in Fig. ~~10~~9. Fig. ~~10a~~9a shows the evolution of summer I_{net} for a pixel in central-western Europe, with a ΔRI_{net} of ~~300~~100 mm ~~year~~month^{-1} (for IPSL-CM6A-LR, randomly chosen GCM). During the baseline period, summer I_{net} fluctuates between zero and about ~~100~~35 mm ~~year~~month^{-1}, while at the end of the century, the maximum I_{net} of the time window will reach ~~400~~135 mm ~~year~~ month^{-1} for SSP5-8.5 with the same minimum I_{net} as for the baseline. For the second pixel in southern Europe (Fig. ~~10b~~9b), a stabilization of the yearly summer requirement is expected. Overall, more water will be required here, but summer I_{net} will not vary importantly relative to the average requirement from one year to another. This second location results in a decrease in RI_{net} of about ~~170~~55 mm ~~year~~month^{-1} for the presented GCM under SSP5-8.5.

25

5 Discussion

5.1 A new model setup for climate change impact assessment

The regional setup of the AquaCrop model using ISIMIP3 meteorological data has potential to assess impacts of climate change on the irrigation requirement and possibly also on future crop production. First, the ~~model~~short-term evaluation proved that the model has an acceptable performance, i.e. the ubRMSD between SIM1 SSM simulations with reanalysis meteorology (ISIMIP3a), and satellite retrievals is 0.06 and 0.08 m³m⁻³, for SMAP and SMOS, respectively (Table ~~1~~3). The lower model performance compared to SMOS SSM could be due to remaining radio frequency interference contamination (Oliva et al., 2012). It is important to note that the satellite target uncertainty is 0.04 m³m⁻³ over areas with less than 5 kg m⁻² vegetation water (i.e. excluding dense vegetation; Entekhabi et al., 2014). Even though a conservative screening was used, this target may be ~~possibly~~ exceeded at some times and locations. The findings of the evaluation against SMAP SSM are comparable to the results found by de Roos et al. (2021). ~~The latter study, however,~~However, the latter study used Modern-Era Restrospective analysis for Research and Applications (version 2) input and showed a slightly higher performance between the simulated SSM of the regional AquaCrop model and SMAP SSM. ~~The~~Furthermore, the difference in study domain and especially in resolution play a major role in explaining this difference (larger domain and soil characteristics aggregated to coarser pixels in this study).

The strong agreement between the SIM2 SSM climatologies obtained with GCM-driven input (ISIMIP3b~~),~~) and the reference satellite ~~and reanalysis driven~~ SSM climatologies (Fig. ~~4~~2), further ~~showed~~confirmed that the historical GCM-driven input is also reliable. A larger bias was observed in wetter moisture conditions (Fig. ~~5~~3), possibly coming from the model itself or from biases in satellite retrievals. Overall, the provided simulated atmospheric data could represent the main variations of SSM for the past (~~2011~~2015-2020) and is therefore reliable to be used for climate change assessments.

The model simulations for the historical evaluation did not include any irrigation and therefore, some mismatches in SSM could possibly be expected in areas which are currently irrigated. Earlier studies suggest that the contrast between satellite observations and model simulation could identify ~~unmodeled~~unmodelled processes (Brocca et al., 2018). In a separate analysis (not shown), this effect was assessed by evaluating the correlation values with regard to irrigation areas that are equipped for irrigation (AEI; similar to de Roos et al., 2021). By using the FAO global maps of irrigated areas version 5 (Siebert et al., 2013) aggregated to ISIMIP resolution, pixels were divided into two groups: (1) less than 10% of the area is equipped for irrigation, and (2) more than 10% of the pixel is equipped. The correlations between AquaCrop SIM1 SSM and satellite SSM for the irrigated pixels (AEI>10%) were nearly identical to correlations for the locations with an AEI<10% (0.65 versus 0.67 for SMOS, and 0.51 for both classes of AEI for SMAP), therefore not revealing where irrigation was missing in the simulations. Even if irrigation could be captured by observation-based SSM (Kim et al., 2020), the low amount of reference satellite data in regions presenting high percentages of AEI compromised the evaluation in this study. The use of a conservative screening of satellite SSM retrievals for both SMOS and SMAP resulted in a significant amount of data loss, especially in densely vegetated areas which are generally masked out (Kim et al., 2020). Further, irrigated areas are usually much smaller than the

considered 0.5º pixel size of this and a recent study. stressed the low potential to detect irrigation at coarse resolutions (Dari et al., 2021). Nevertheless, the second time series presented in Fig. 3b1b showed an underestimation of SSM during summer by the model and large differences between SMOS and SMAP, both suggesting potential irrigation applications, as confirmed by

540   a high AEI percentage.

5.2 Future mean and interannual variability of summer I_{net}

The evolution of future summer I_{net} with climate change is highly dependent on the scenario (SSP), but also on the GCM (Table 24, Fig. 6). This agrees4). Our results agree with several earlier droughts and irrigation projection assessments (Döll, 2002; Elliott et al., 2014; Konzmann et al., 2013; Pfister et al., 2011; Pokhrel et al., 2021; Ruosteenoja et al., 2018; Satoh et

545   al., 2021; Schaldach et al., 2012; Wada et al., 2013). Under high and extreme emission scenarios, the whole continent will be significantly impacted by the end of the century (Fig. 7e5e and f), with the most drastic changes in central and upper southern latitudes of the study domain, confirmed by the high increases in meteorological (Spinoni et al., 2018) and soil water (Ruosteenoja et al., 2018) shortages in these regions. ΔI_{net} spatial patterns (Fig. 75) are comparable to the findings of Konzmann et al. (2013) and Wada et al. (2013) for the most affected areas where all GCMs present significant changes. Eastern Europe

550   shows on average large positive ΔI_{net} values but not all GCMs converge towards significant changes in this region. Moreover, the model evaluation showed a lower performance over this area (Fig. 3a1a). For these two reasons, the results may be less certain. Absolute

For the year 2050, Schadlach et al. (2013) estimated an average increase of 70 mm year^{-1} (+15% compared to the baseline of 470 mm year^{-1}) of the I_{net} over the European continent under a high emission scenario. For the same scenario, Fischer et al.

555   (2007) predicted an increase of 53 mm year^{-1} (+36% compared to the baseline of 147 mm year^{-1}) over western Europe by 2080. These values are comparable to the results of this study, presenting a mean increase of 38 mm year^{-1} (+17% compared to the baseline of 221 mm year^{-1}, integrated over the three summer months only) and 67 mm year^{-1} (+30%) for 2050 and 2090, respectively, and for a comparable emission scenario (SSP3-7.0). Also, the evolution of I_{net} under SSP5-8.5 (+35%) can be related to the findings from Wada et al. (2013) for which increases larger than 25% are estimated over almost the entire

560   European continent. Under this same scenario, the results show that France will face extreme increases in I_{net} (+75%) confirmed by Fader et al. (2016) (+80%). Smaller increases were found in other studies (e.g., Döll, 2002; Elliott et al., 2014), however absolute values are hard to directly confront to literature because of the differences in methodology compared to other studies. In literature, I_{net} is often assessed under the assumption of potential irrigation during the entire year or growing season (as opposed to the summer only in this study), considering other factors such as irrigation efficiencies and strategies, varying crop

565   types, and even population increase or economic growth ultimately impacting e.g. irrigation efficiencies. FurthermoreFurthermore, Elliott et al. (2014) demonstrated that irrigation estimates from GHMs deviate strongly from crop model predictions, potentially due to the differences in agrohydrological processes between the two types of models. Also, Wada et al. (2013) proved that the largest part of uncertainty in future I_{net} estimation is due to the impact model in the first

27

place, and only then to climate uncertainty. ET_0 is a determinant factor for these kinds of studies, and its calculation procedures can have an important influence on the final results (Webber et al., 2016).

Atmospheric data alone could give an indication of the crop water requirement, as is done in meteorological drought assessments. However, the integration of P and ET_0 into a crop model with application of irrigation is more realistic to estimate I_{net}, because it benefits from the land system memory. It should be noted though that the wetness of the irrigated land area will in turn affect turbulent fluxes and thus atmospheric variables in general (Hirsch et al., 2017; Thiery et al., 2017; 2020; Keune et al., 2018). This feedback loop is not included in the presented simulations and needs to be carefully considered in future attempts to design climate-smart irrigation systems.

Whereas the focus of this study was on the irrigation requirement, a similar analysis can be performed in terms of agricultural productivity. An increase in I_{net} is expected but, following increasing CO_2 concentrations, biomass production is also expected to increase (Schleussner et al., 2018; Vanuytrecht, 2020; Vanuytrecht et al., 2012). The yield water productivity ($WP_{Y/ET}$, i.e. the ratio between crop yield and the amount of water lost by evapotranspiration) will improve due to the rising CO_2 concentrations. Since crops can only fully profit of the CO_2 fertilization when soil fertility is high (Raes et al., 2021), an increase in $WP_{Y/ET}$ is likely to occur in irrigated fields that are generally well fertilized. In the absence of soil water and soil fertility stress, crop production might increase by about 25% up to 45% for an atmospheric CO_2 concentration of 550 ppm (Raes et al., 2017). Effects above this concentration remain more uncertain.

5.3 Future adaptations of irrigation infrastructure and management

Different practical future pathways can be considered starting from the current state of irrigation requirement. In regions where I_{net} is currently low (low baseline I_{net}), there is typically no irrigation infrastructure available or needed to achieve a fairly high crop production. However, to maintain crop production in the future, large investments will be required to develop or extend the irrigation infrastructure (Rosa et al., 2020). In regions with an existing water shortage and irrigation infrastructure, the focus will be on improving irrigation efficiencies, aiming to buffer the effects of climate change (Jägermeyr et al., 2016). Our study did not consider specific irrigation practices and efficiencies. The latter have been estimated around 50% in Europe (Fischer et al., 2007; Rohwer et al., 2007; Wada et al., 2013), meaning that the I_{net} values presented in this study could roughly be doubled to obtain the gross requirement. Sprinkler irrigation remains the most widely used practice in Europe, but the share of drip irrigation is progressively increasing in southern countries such as Spain and Italy (Monaghan et al., 2013), aiming at improving irrigation efficiencies. Furthermore, with a lower availability of freshwater, the introduction of other irrigation strategies, such as deficit irrigation, also gains importance. Deficit irrigation intends to maximize crop water productivity, therefore stabilizing crop yields through time (Geerts and Raes, 2009; Mushtaq and Moghaddasi, 2011).

5.4 Model uncertainty

Model uncertainty is an important factor influencing climate scenario analysisanalyses (Lehner et al., 2020). This starts with the high variability between climate scenarios that are input to the crop model simulations. The uncertainty of future climate

28

was included by using meteorological input from three scenarios and five GCMs, resulting in 15 different SSP-GCM combinations. The process of using only a small fraction of the various existing GCMs has been criticized (McSweeney and Jones, 2016). However, previous drought and irrigation projections often used less than five GCMs or used more but for only one emission scenario. Additionally, the ISIMIP GCMs are carefully selected to represent the entire CMIP ensemble (Frieler
605 et al., 2017; Warszawski et al., 2014).

The AquaCrop model setup also adds uncertainty. First, the constantly evolving field practices in terms of e.g. crop type and cultivars, water management, and soil fertility management were not included in the model simulations. However, this aspect is almost impossible to include. Second, the model generalizations (generic C3-type of crop, unconstrained water availability and constant small soil fertility stress for the whole domain) increase the uncertainty in the projections. It should be noted that
610 actual area of irrigated land is not considered, and consequently, the expansion thereof is not simulated (estimated by e.g. Schaldach et al., 2012). Nevertheless, the intention of this study ~~aimed~~is to limit the uncertainty in time and space (as described in section 2.2) by assuming these generalizations, therefore aiming to present in a simple way the evolution of I_{net} during summer months~~, despite these generalisations in time and space~~.

6 Conclusions

615 Large-scale AquaCrop simulations over Europe were performed using ISIMIP3 meteorological forcings at a spatial resolution of 0.5° lat x 0.5° lon to assess future changes in net irrigation requirements~~. The~~ I_{net}. Because this is the first large-scale AquaCrop application with ISIMIP3 input, the model was first evaluated using satellite-based SSM ~~to evaluate the skill of AquaCrop SSM forced with historical ISIMIP3 reanalysis and GCM-based meteorology.~~. The reanalysis-driven (ISIMIP3a) simulated SSM have a mean spatial ubRMSD of 0.06 m³m^{-3} with SMAP retrievals, and thereby deviate slightly more than the
620 assumed intrinsic error of the satellite retrieval error (0.04 m³m^{-3}). The performance of AquaCrop compared with SMOS (ubRMSD=0.08 m³m^{-3}) is slightly lower than with SMAP, most likely ~~due to~~because the ~~older~~SMOS sensor ~~of SMOS which~~ suffers more from radio frequency interference. When using GCM-driven (ISIMIP3b) meteorology as input, the ~~resulting simulated~~multi-year average SSM ~~climatologies for~~ of the ~~years 2011 through 2020 agree closely with the SSM climatology of the reanalysis product. In addition, GCM driven SSM climatologies are~~simulations is comparable to that of reference
625 satellite ~~climatologies~~data (ubRMSD=0.03 m³m^{-3}), which reinforces the reliability of the ISIMIP3 climate data for future projections.

In the second part of this paper, the summer irrigation requirement of a near- (2031-2060) and far- (2071-2100) future horizon was simulated using five different GCMs and three emissions scenarios. We present net irrigation requirement values that are independent of the irrigated area, period, infrastructure and the exact crop type. The mean and interannual variability in net
630 irrigation requirement I_{net} for the summer months were quantified for the two future climate horizons and compared to the baseline period (1985-2014). This evaluation showed that the effect of climate change on future I_{net} depends on the emission scenario, but more strongly on the GCM. Under high and extreme emission scenarios (SSP3-7.0 and SSP5-8.5), almost the

whole European continent will see an increase in summer I_{net}, with on average 30% and 35% additional net irrigation water required in the far future relative to the baseline I_{net}. Especially regions with a moderate baseline I_{net} will experience strong

635 increases in I_{net}. All GCMs agree on significant increases in central to southern Europe, which is in line with meteorological and soil moisture drought projections for the same scenarios, as well as previous irrigation demand projections.

The interannual variability in summer I_{net} was quantified by the range between maximum and minimum I_{net} within the 30-year climate periods, RI_{net}. It was found that mild increases in I_{net} result in larger gaps between maximum and minimum summer I_{net} within a time window, corresponding to more extremes, and a high interannual variability (large RI_{net}). In the future,

640 northern and central areas will face increased RI_{net}, whereas southern Europe is likely to see the variability diminish resulting in steady high I_{net}. Under the strong mitigation scenario (SSP1-2.6), I_{net} stabilizes towards the end of the century, consistent with the plateauing CO_2 concentrations in this scenario. The increase in variability is also reduced under this scenario. Overall, extra water will be required, but more production can be achieved under higher CO_2 concentrations. The exact effect of CO_2 fertilization remains uncertain, but it is expected that yield, and especially yield water productivity, are likely to increase in

645 the future in absence of water and soil fertility stress. Our large-scale setup with AquaCrop is well suited to explore the effect of climate scenarios on crop productivity in future research.

These results highlight the importance of climate change mitigation to keep future irrigation at reasonable levels, while it also stresses the high uncertainty of climate projections. This study aimed to demonstrate the effect of climate change on I_{net} over Europe, without considering land use, crop types, and actual irrigated areas to avoid the inclusion of more uncertainty.

650 Therefore, the results of this study should not be taken as predictions but as an indication of the potential consequences of climate change on the amount and variability of I_{net} for the summer months.

Appendices

Appendix A: comparison of SIM1 and SMOS SSM in terms of anomalies

To evaluate the short-term and interannual variability in the AquaCrop SSM in terms of temporal anomaly correlation

655 (anomR), time series of anomalies are calculated by subtracting the climatology from simulation and satellite data for each daily time step. The climatology calculates the mean seasonal cycle as a long-term mean using a sliding window of 31 days with a minimum threshold of three data points of data within the window.

Because anomR values can only be computed when several years of data are available, the AquaCrop SSM simulations forced with ISIMIP3a reanalysis data for the years 2011-2016 (SIM1) are evaluated against SMOS SSM retrievals only. Figure A1

660 shows the anomR over Europe with a spatial mean anomR of 0.44. Higher correlations are found in south-western locations (anomR often > 0.6) and lower performances occur in north and central-western Europe (anomR generally < 0.4). Also shown on this figure is a partitioning of Europe in various zones for further discussion.
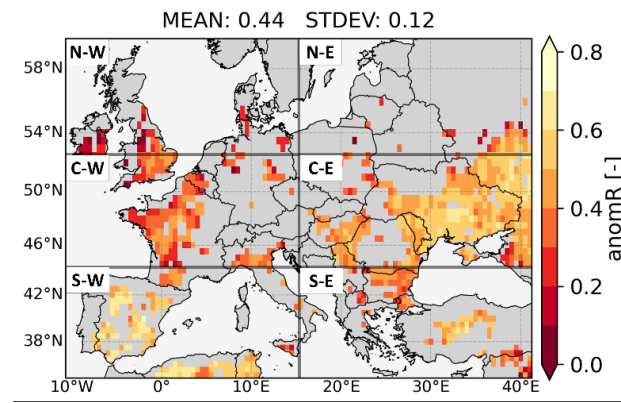
Figure A1 Anomaly correlation (anomR) between SIM1 AquaCrop SSM and SMOS SSM for the period 2011-2016. The spatial mean and standard deviation are indicated (MEAN, STDEV). The six European sub-regions used to describe the model evaluation and the future I_{net} are indicated (from top left to bottom right: north-west, north-east, central-west, central-east, south-west, south-east).

Code and data availability

The~~All results (metrics from the model evaluation, I~~net~~ and RI~~net~~ for the three time windows) can be provided in netCDF format by contacting the authors. The original~~ regional AquaCrop (v6.1) is available on Zenodo at https://doi.org/10.5194/gmd-2021-98 (de Roos et al., 2021). ISIMIP input data can be retrieved from https://www.isimip.org/gettingstarted/input-data-bias-correction/. The ~~Python code and~~ other input datasets and Python code for the complete setup of this specific research can be obtained by contacting the authors. All results (metrics from the model evaluation, I_{net} and RI_{net} for the three time windows) can be provided in netCDF format by contacting the authors. The netCDF files and model setup will be publicly available after the acceptance of this paper.

Author contributions

LB adapted the code to run the regional version of AquaCrop with ISIMIP data, prepared the input data, conducted the model evaluation, performed all simulations and analyses. SDR provided the code of the regional version of AquaCrop (v6.1) and scientific guidance. GDL prioritized the main steps taken in the paper, provided supervision and scientific guidance throughout all research advances, and manages HPC usage. WT provided scientific guidance through climate change impact assessments and ISIMIP. DR provided scientific guidance regarding the use and interpretation of AquaCrop, along with an appropriate methodology to assess future irrigation requirements. LB wrote the paper and all authors contributed.

Competing interests

The authors declare that they have no conflict of interests.

References

Albergel, C., Dorigo, W., Reichle, R. H., Balsamo, G., Rosnay, P. de, Muñoz-Sabater, J., Isaksen, L., Jeu, R. de, and Wagner, W.: Skill and Global Trend Analysis of Soil Moisture from Reanalyses and Microwave Remote Sensing, J. Hydrometeorol., 14, 1259–1277, https://doi.org/10.1175/JHM-D-12-0161.1, 2013.

Allen, R. G., Pereira, L. S., Raes, D., and Smith, M.: Crop evapotranspiration, Irrig. Drainage Paper, 56, Rome, Italy: UN Food and Agriculture Organization, 1998

Balkovič, J., van der Velde, M., Schmid, E., Skalský, R., Khabarov, N., Obersteiner, M., Stürmer, B., and Xiong, W.: Pan-European crop modelling with EPIC: Implementation, up-scaling and regional crop yield validation, Agr. Syst., 120, 61–75, https://doi.org/10.1016/j.agsy.2013.05.008, 2013.

Bondeau, A., Smith, P. C., Zaehle, S., Schaphoff, S., Lucht, W., Cramer, W., Gerten, D., Lotze-Campen, H., Müller, C., Reichstein, M., and Smith, B.: Modelling the role of agriculture for the 20th century global terrestrial carbon balance, Glob. Change. Biol., 13, 679–706, https://doi.org/10.1111/j.1365-2486.2006.01305.x, 2007.

Boogaard, H., Wolf, J., Supit, I., Niemeyer, S., and van Ittersum, M.: A regional implementation of WOFOST for calculating yield gaps of autumn-sown wheat across the European Union, Field Crop. Res., 143, 130–142, https://doi.org/10.1016/j.fcr.2012.11.005, 2013.

Boulange, J., Hanasaki, N., Satoh, Y., Yokohata, T., Shiogama, H., Burek, P., Thiery, W., Gerten, D., Schmied, H. M., Wada, Y., Gosling, S. N., Pokhrel, Y., and Wanders, N.: Validity of estimating flood and drought characteristics under equilibrium climates from transient simulations, Environ. Res. Lett., 16, 104028, https://doi.org/10.1088/1748-9326/ac27cc, 2021.

Brauman, K. A., Siebert, S., and Foley, J. A.: Improvements in crop water productivity increase water sustainability and food security—a global analysis, Environ. Res. Lett., 8, 024030, https://doi.org/10.1088/1748-9326/8/2/024030, 2013.

Brocca, L., Tarpanelli, A., Filippucci, P., Dorigo, W., Zaussinger, F., Gruber, A., and Fernández-Prieto, D.: How much water is used for irrigation? A new approach exploiting coarse resolution satellite soil moisture products, Int. J. Appl. Earth Obs. 73, 752–766, https://doi.org/10.1016/j.jag.2018.08.023, 2018.

Chan, S. K., Bindlish, R., O'Neill, P. E., Njoku, E., Jackson, T., Colliander, A., Chen, F., Burgin, M., Dunbar, S., Piepmeier, J., Yueh, S., Entekhabi, D., Cosh, M. H., Caldwell, T., Walker, J., Wu, X., Berg, A., Rowlandson, T., Pacheco, A., McNairn, H., Thibeault, M., Martínez-Fernández, J., González-Zamora, Á., Seyfried, M., Bosch, D., Starks, P., Goodrich, D., Prueger, J., Palecki, M., Small, E. E., Zreda, M., Calvet, J.-C., Crow, W. T., and Kerr, Y.: Assessment of the SMAP Passive Soil Moisture Product, IEEE T. Geosci. Remote, 54, 4994–5007, https://doi.org/10.1109/TGRS.2016.2561938, 2016.

Chiarelli, D. D., Passera, C., Rosa, L., Davis, K. F., D'Odorico, P., and Rulli, M. C.: The green and blue crop water requirement WATNEEDS model and its global gridded outputs, Sci Data, 7, 273, https://doi.org/10.1038/s41597-020-00612-0, 2020.

Cucchi, M., Weedon, G. P., Amici, A., Bellouin, N., Lange, S., Müller Schmied, H., Hersbach, H., and Buontempo, C.: WFDE5: bias-adjusted ERA5 reanalysis data for impact studies, Earth Syst. Sci. Data, 12, 2097–2120, https://doi.org/10.5194/essd-12-2097-2020, 2020.

Dale, A., Fant, C., Strzepek, K., Lickley, M., and Solomon, S.: Climate model uncertainty in impact assessments for agriculture: A multi-ensemble case study on maize in sub-Saharan Africa, Earth's Future, 5, 337–353, https://doi.org/10.1002/2017EF000539, 2017.

Dari, J., Quintana-Seguí, P., Escorihuela, M. J., Stefan, V., Brocca, L., and Morbidelli, R.: Detecting and mapping irrigated areas in a Mediterranean environment by using remote sensing soil moisture and a land surface model, Journal of Hydrology, 596, 126129, https://doi.org/10.1016/j.jhydrol.2021.126129, 2021.

De Lannoy, G. J. M. and Reichle, R. H.: Assimilation of SMOS brightness temperatures or soil moisture retrievals into a land surface model, Hydrol. Earth Syst. Sci., 20, 4895–4911, https://doi.org/10.5194/hess-20-4895-2016, 2016.

De Lannoy, G. J. M., Koster, R. D., Reichle, R. H., Mahanama, S. P. P., and Liu, Q.: An updated treatment of soil texture and associated hydraulic properties in a global land modeling system, J. Adv. Model. Earth Sy., 6, 957–979, https://doi.org/10.1002/2014MS000330, 2014.

de Roos, S., De Lannoy, G. J. M., and Raes, D.: Performance analysis of regional AquaCrop (v6.1) biomass and surface soil moisture simulations using satellite and in situ observations, Geosci. Model Dev., 14, 7309–7328, https://doi.org/10.5194/gmd-14-7309-2021, 2021.

de Roos, S., De Lannoy, G., and Raes, D.: source code and datasets for gmd-2021-98, Version 1, Zenodo [data set], https://doi.org/10.5281/zenodo.4770738, 2021

de Wit, A. J. W. and van Diepen, C. A.: Crop model data assimilation with the Ensemble Kalman filter for improving regional crop yield forecasts, Agr. Forest Meterol., 146, 38–56, https://doi.org/10.1016/j.agrformet.2007.05.004, 2007.

Dirmeyer, P. and Oki, T.: The Second Global Soil Wetness project (GSWP-2) Science 2 and Implementation Plan, International GEWEX Project Office Publication (IGPO), Columbia, Md, IGPO Publication Series No. 37, 64 pp., 2002.

Döll, P.: Impact of Climate Change and Variability on Irrigation Requirements: A Global Perspective, Climatic Change, 54, 269–293, https://doi.org/10.1023/A:1016124032231, 2002.

Döll, P. and Siebert, S.: Global modeling of irrigation water requirements, Water Resour. Res., 38, 8-1-8–10, https://doi.org/10.1029/2001WR000355, 2002.

Elliott, J., Deryng, D., Müller, C., Frieler, K., Konzmann, M., Gerten, D., Glotter, M., Flörke, M., Wada, Y., Best, N., Eisner, S., Fekete, B. M., Folberth, C., Foster, I., Gosling, S. N., Haddeland, I., Khabarov, N., Ludwig, F., Masaki, Y., Olin, S., Rosenzweig, C., Ruane, A. C., Satoh, Y., Schmid, E., Stacke, T., Tang, Q., and Wisser, D.: Constraints and potentials of future

irrigation water availability on agricultural production under climate change, P. Natl. Acad. Sci. USA, 111, 3239–3244, https://doi.org/10.1073/pnas.1222474110, 2014.

Entekhabi, D., Yueh, S., O'Neill, P., Kellogg, K. H., Allen, A., Bindlish, R., Brown, M., Chan, S., Colliander, A., Crow, W. T, Das, N., De Lannoy, G., Dunbar, R. S., Edelstein, W. N., Entin, J. K., Escobar, V., Goodman, S. D., Jackson, T. J., Jai, B., Johnson, J., Kim, E., Kim, S., Kimball, J., Koster, R. D., Leon, A., McDonald, K. C., Moghaddam, M., Mohammed, P., Moran, S., Njoku, E. G., Piepmeier, J. R., Reichle, R., Rogez, F., Shi, J. C., Spencer, M. W., Thurman, S. W., Tsang, L., Van Zyl, J., Weiss, B., and West, R.: SMAP Handbook–soil moisture active passive: Mapping soil moisture and freeze/thaw from space, JPL publication, Pasadena, California USA, 192 pp., JPL 400-1567, 2014.

Fader, M., Shi, S., von Bloh, W., Bondeau, A., and Cramer, W.: Mediterranean irrigation under climate change: more efficient irrigation needed to compensate for increases in irrigation water requirements, Hydrol. Earth Syst. Sci., 20, 953–973, https://doi.org/10.5194/hess-20-953-2016, 2016.

Fischer, G., Tubiello, F. N., van Velthuizen, H., and Wiberg, D. A.: Climate change impacts on irrigation water requirements: Effects of mitigation, 1990–2080, Technol. Forecast Soc., 74, 1083–1107, https://doi.org/10.1016/j.techfore.2006.05.021, 2007.

Foster, T., Brozović, N., Butler, A. P., Neale, C. M. U., Raes, D., Steduto, P., Fereres, E., and Hsiao, T. C.: AquaCrop-OS: An open source version of FAO's crop water productivity model, Agr. Water Manage., 181, 18–22, https://doi.org/10.1016/j.agwat.2016.11.015, 2017.

Frieler, K., Lange, S., Piontek, F., Reyer, C. P. O., Schewe, J., Warszawski, L., Zhao, F., Chini, L., Denvil, S., Emanuel, K., Geiger, T., Halladay, K., Hurtt, G., Mengel, M., Murakami, D., Ostberg, S., Popp, A., Riva, R., Stevanovic, M., Suzuki, T., Volkholz, J., Burke, E., Ciais, P., Ebi, K., Eddy, T. D., Elliott, J., Galbraith, E., Gosling, S. N., Hattermann, F., Hickler, T., Hinkel, J., Hof, C., Huber, V., Jägermeyr, J., Krysanova, V., Marcé, R., Müller Schmied, H., Mouratiadou, I., Pierson, D., Tittensor, D. P., Vautard, R., van Vliet, M., Biber, M. F., Betts, R. A., Bodirsky, B. L., Deryng, D., Frolking, S., Jones, C. D., Lotze, H. K., Lotze-Campen, H., Sahajpal, R., Thonicke, K., Tian, H., and Yamagata, Y.: Assessing the impacts of 1.5 °C global warming – simulation protocol of the Inter-Sectoral Impact Model Intercomparison Project (ISIMIP2b), Geosci. Model Dev., 10, 4321–4345, https://doi.org/10.5194/gmd-10-4321-2017, 2017.

Geerts, S. and Raes, D.: Deficit irrigation as an on-farm strategy to maximize crop water productivity in dry areas, Agr. Water Manage., 96, 1275–1284, https://doi.org/10.1016/j.agwat.2009.04.009, 2009.

Greve, P., Orlowsky, B., Mueller, B., Sheffield, J., Reichstein, M., and Seneviratne, S. I.: Global assessment of trends in wetting and drying over land, Nat. Geosci, 7, 716–721, https://doi.org/10.1038/ngeo2247, 2014.

Grillakis, M. G.: Increase in severe and extreme soil moisture droughts for Europe under climate change, Sci. Total Environ., 660, 1245–1255, https://doi.org/10.1016/j.scitotenv.2019.01.001, 2019.

Gudmundsson, L., Boulange, J., Do, H. X., Gosling, S. N., Grillakis, M. G., Koutroulis, A. G., Leonard, M., Liu, J., Müller Schmied, H., Papadimitriou, L., Pokhrel, Y., Seneviratne, S. I., Satoh, Y., Thiery, W., Westra, S., Zhang, X., and Zhao, F.: Globally observed trends in mean and extreme river flow attributed to climate change, Science, 371, 1159–1162, https://doi.org/10.1126/science.aba3996, 2021.

Haddeland, I., Heinke, J., Biemans, H., Eisner, S., Flörke, M., Hanasaki, N., Konzmann, M., Ludwig, F., Masaki, Y., Schewe, J., Stacke, T., Tessler, Z. D., Wada, Y., and Wisser, D.: Global water resources affected by human interventions and climate change, P. Natl. Acad. Sci. USA, 111, 3251–3256, https://doi.org/10.1073/pnas.1222475110, 2014.

Hirsch, A. L., Wilhelm, M., Davin, E. L., Thiery, W., and Seneviratne, S. I.: Can climate-effective land management reduce regional warming?, J. Geophys. Res.-Atmos.,122, 2269–2288, https://doi.org/10.1002/2016JD026125, 2017.

795 Hurtt, G. C., Chini, L., Sahajpal, R., Frolking, S., Bodirsky, B. L., Calvin, K., Doelman, J. C., Fisk, J., Fujimori, S., Klein Goldewijk, K., Hasegawa, T., Havlik, P., Heinimann, A., Humpenöder, F., Jungclaus, J., Kaplan, J. O., Kennedy, J., Krisztin, T., Lawrence, D., Lawrence, P., Ma, L., Mertz, O., Pongratz, J., Popp, A., Poulter, B., Riahi, K., Shevliakova, E., Stehfest, E., Thornton, P., Tubiello, F. N., van Vuuren, D. P., and Zhang, X.: Harmonization of global land use change and management for the period 850–2100 (LUH2) for CMIP6, 13, 5425–5464, https://doi.org/10.5194/gmd-13-5425-2020, 2020.

IPCC, Climate Change 2021: The Physical Science Basis. Contribution of Working Group I to the Sixth Assessment Report
800 of the Intergovernmental Panel on Climate Change, edited by: Masson-Delmotte, V., Zhai, P., Pirani, A., Connors, S. L., Péan, C., Berger, S., Caud, N., Chen, Y., Goldfarb, L., Gomis, M. I., Huang, M., Leitzell, K., Lonnoy, E., Matthews, J. B. R., Maycock, T. K., Waterfield, T., Yelekçi, Ö., Yu, R., and Zhou, B., Cambridge University Press, 2021.

Jägermeyr, J., Gerten, D., Schaphoff, S., Heinke, J., Lucht, W., and Rockström, J.: Integrated crop water management might sustainably halve the global food gap, Environ. Res. Lett., 11, 025002, https://doi.org/10.1088/1748-9326/11/2/025002, 2016.

805 Jägermeyr, J., Müller, C., Ruane, A. C., Elliott, J., Balkovic, J., Castillo, O., Faye, B., Foster, I., Folberth, C., Franke, J. A., Fuchs, K., Guarin, J. R., Heinke, J., Hoogenboom, G., Iizumi, T., Jain, A. K., Kelly, D., Khabarov, N., Lange, S., Lin, T.-S., Liu, W., Mialyk, O., Minoli, S., Moyer, E. J., Okada, M., Phillips, M., Porter, C., Rabin, S. S., Scheer, C., Schneider, J. M., Schyns, J. F., Skalsky, R., Smerald, A., Stella, T., Stephens, H., Webber, H., Zabel, F., and Rosenzweig, C.: Climate impacts on global agriculture emerge earlier in new generation of climate and crop models, Nat Food, 2, 873–885,
810 https://doi.org/10.1038/s43016-021-00400-y, 2021.

Kerr, Y. H., Waldteufel, P., Wigneron, J.-P., Delwart, S., Cabot, F., Boutin, J., Escorihuela, M.-J., Font, J., Reul, N., Gruhier, C., Juglea, S. E., Drinkwater, M. R., Hahne, A., Martín-Neira, M., and Mecklenburg, S.: The SMOS Mission: New Tool for Monitoring Key Elements ofthe Global Water Cycle, IEEE, 98, 666–687, https://doi.org/10.1109/JPROC.2010.2043032, 2010.

Keune, J., Sulis, M., Kollet, S., Siebert, S., and Wada, Y.: Human Water Use Impacts on the Strength of the Continental Sink
815 for Atmospheric Water, Geophys. Res. Lett., 45, 4068–4076, https://doi.org/10.1029/2018GL077621, 2018.

Kim, H., Wigneron, J.-P., Kumar, S., Dong, J., Wagner, W., Cosh, M. H., Bosch, D. D., Collins, C. H., Starks, P. J., Seyfried, M., and Lakshmi, V.: Global scale error assessments of soil moisture estimates from microwave-based active and passive satellites and land surface models over forest and mixed irrigated/dryland agriculture regions, Proc. SPIE, 251, 112052, https://doi.org/10.1016/j.rse.2020.112052, 2020.

820 King, M., Altdorff, D., Li, P., Galagedara, L., Holden, J., and Unc, A.: Northward shift of the agricultural climate zone under 21st-century global climate change, Sci Rep, 8, 7904, https://doi.org/10.1038/s41598-018-26321-8, 2018.

Konzmann, M., Gerten, D., and Heinke, J.: Climate impacts on global irrigation requirements under 19 GCMs, simulated with a vegetation and hydrology model, Hydrolog. Sci. J., 58, 88–105, https://doi.org/10.1080/02626667.2013.746495, 2013.

Lange, S.: WFDE5 over land merged with ERA5 over the ocean (W5E5) (1.0), GFZ Data Services,
825 https://doi.org/10.5880/PIK.2019.023, 2019a.

Lange, S.: Trend-preserving bias adjustment and statistical downscaling with ISIMIP3BASD (v1.0), Geosci. Model Dev., 12, 3055–3070, https://doi.org/10.5194/gmd-12-3055-2019, 2019b.

Lange, S.: ISIMIP3BASD (2.4.1), Zenodo, https://doi.org/10.5281/ZENODO.3898426, 2020.

830 Lange, S., Volkholz, J., Geiger, T., Zhao, F., Vega, I., Veldkamp, T., Reyer, C. P. O., Warszawski, L., Huber, V., Jägermeyr, J., Schewe, J., Bresch, D. N., Büchner, M., Chang, J., Ciais, P., Dury, M., Emanuel, K., Folberth, C., Gerten, D., Gosling, S. N., Grillakis, M., Hanasaki, N., Henrot, A.-J., Hickler, T., Honda, Y., Ito, A., Khabarov, N., Koutroulis, A., Liu, W., Müller, C., Nishina, K., Ostberg, S., Müller Schmied, H., Seneviratne, S. I., Stacke, T., Steinkamp, J., Thiery, W., Wada, Y., Willner, S., Yang, H., Yoshikawa, M., Yue, C., and Frieler, K.: Projecting Exposure to Extreme Climate Impact Events Across Six Event Categories and Three Spatial Scales, Earth's Future, 8, e2020EF001616, https://doi.org/10.1029/2020EF001616, 2020.

835 Leggett, J., Pepper, W. J., Swart, R. J., Edmonds, J., Meira Filho, L. G., Mintzer, I., and Wang, M. X.: Emissions scenarios for the IPCC: an update, Climate Change, 1040, 75–95, 1992.

Lehner, F., Deser, C., Maher, N., Marotzke, J., Fischer, E. M., Brunner, L., Knutti, R., and Hawkins, E.: Partitioning climate projection uncertainty with multiple large ensembles and CMIP5/6, Earth Syst. Dynam., 11, 491–508, https://doi.org/10.5194/esd-11-491-2020, 2020.

840 Liu, J. and Yang, H.: Spatially explicit assessment of global consumptive water uses in cropland: Green and blue water, Journal of Hydrology, 384, 187–197, https://doi.org/10.1016/j.jhydrol.2009.11.024, 2010.

Mahanama, S. P., Koster, R. D., Walker, G. K., Tackacs, L., Reichle, R. H., De Lannoy, G., Liu, Q., Zhao, B., and Suarez, M.: Land Boundary Conditions for the Goddard Earth Observing System Model Version 5 (GEOS-5) Climate Modeling System – Recent Updates and Data File Descriptions, NASA Technical Report Series on Global Modeling and Data Assimilation 104606, Vol. 39, NASA Goddard Space Flight Center, MD, USA, 51 pp., 2015.

845 Massari, C., Modanesi, S., Dari, J., Gruber, A., De Lannoy, G. J. M., Girotto, M., Quintana-Seguí, P., Le Page, M., Jarlan, L., Zribi, M., Ouaadi, N., Vreugdenhil, M., Zappa, L., Dorigo, W., Wagner, W., Brombacher, J., Pelgrum, H., Jaquot, P., Freeman, V., Volden, E., Fernandez Prieto, D., Tarpanelli, A., Barbetta, S., and Brocca, L.: A Review of Irrigation Information Retrievals from Space and Their Utility for Users, Remote Sens.-Basel., 13, 4112, https://doi.org/10.3390/rs13204112, 2021.

850 McSweeney, C. F. and Jones, R. G.: How representative is the spread of climate projections from the 5 CMIP5 GCMs used in ISI-MIP?, Climate Services, 1, 24–29, https://doi.org/10.1016/j.cliser.2016.02.001, 2016.

Menzel, A. and Fabian, P.: Growing season extended in Europe, 397, 659–659, https://doi.org/10.1038/17709, 1999.

Monaghan, J. M., Daccache, A., Vickers, L. H., Hess, T. M., Weatherhead, E. K., Grove, I. G., and Knox, J. W.: More 'crop per drop': constraints and opportunities for precision irrigation in European agriculture, 93, 977–980, https://doi.org/10.1002/jsfa.6051, 2013.

Monfreda, C., Ramankutty, N., and Foley, J. A.: Farming the planet: 2. Geographic distribution of crop areas, yields, physiological types, and net primary production in the year 2000, 22, https://doi.org/10.1029/2007GB002947, 2008.

Monteith, J. L.: The Quest for Balance in Crop Modeling, Agron. J., 88, 695–697, https://doi.org/10.2134/agronj1996.00021962008800050003x, 1996.

860 Müller, C., Elliott, J., Chryssanthacopoulos, J., Arneth, A., Balkovic, J., Ciais, P., Deryng, D., Folberth, C., Glotter, M., Hoek, S., Iizumi, T., Izaurralde, R. C., Jones, C., Khabarov, N., Lawrence, P., Liu, W., Olin, S., Pugh, T. A. M., Ray, D. K., Reddy, A., Rosenzweig, C., Ruane, A. C., Sakurai, G., Schmid, E., Skalsky, R., Song, C. X., Wang, X., de Wit, A., and Yang, H.: Global gridded crop model evaluation: benchmarking, skills, deficiencies and implications, Geosci. Model Dev., 10, 1403–1422, https://doi.org/10.5194/gmd-10-1403-2017, 2017.

865 Mushtaq, S. and Moghaddasi, M.: Evaluating the potentials of deficit irrigation as an adaptive response to climate change and environmental demand, Environ. Sci. Policy, 14, 1139–1150, https://doi.org/10.1016/j.envsci.2011.07.007, 2011.

Nakicenovic, N., Alcamo, J., Davis, G., Vries, B. de, Fenhann, J., Gaffin, S., Gregory, K., Grubler, A., Jung, T. Y., Kram, T., Rovere, E. L. L., Michaelis, L., Mori, S., Morita, T., Pepper, W., Pitcher, H., Price, L., Riahi, K., Roehrl, A., Rogner, H.-H., Sankovski, A., Schlesinger, M., Shukla, P., Smith, S., Swart, R., Rooijen, S. van, Victor, N., and Zhou, D.: Special report on emissions scenarios, Lawrence Berkeley National Laboratory, LBNL-59940, retrieved from: https://escholarship.org/uc/item/9sz5p22f, 2000.

Niu, G.-Y., Yang, Z.-L., Mitchell, K. E., Chen, F., Ek, M. B., Barlage, M., Kumar, A., Manning, K., Niyogi, D., Rosero, E., Tewari, M., and Xia, Y.: The community Noah land surface model with multiparameterization options (Noah-MP): 1. Model description and evaluation with local-scale measurements, J. Geophys. Res.-Atmos., 116, https://doi.org/10.1029/2010JD015139, 2011.

O'Neill, B. C., Kriegler, E., Riahi, K., Ebi, K. L., Hallegatte, S., Carter, T. R., Mathur, R., and van Vuuren, D. P.: A new scenario framework for climate change research: the concept of shared socioeconomic pathways, Climatic Change, 122, 387–400, https://doi.org/10.1007/s10584-013-0905-2, 2014.

Oliva, R., Daganzo, E., Kerr, Y. H., Mecklenburg, S., Nieto, S., Richaume, P., and Gruhier, C.: SMOS Radio Frequency Interference Scenario: Status and Actions Taken to Improve the RFI Environment in the 1400–1427-MHz Passive Band, IEEE T. Geosci. Remote, 50, 1427–1439, https://doi.org/10.1109/TGRS.2012.2182775, 2012.

Pfister, S., Bayer, P., Koehler, A., and Hellweg, S.: Projected water consumption in future global agriculture: Scenarios and related impacts, Sci. Total Environ., 409, 4206–4216, https://doi.org/10.1016/j.scitotenv.2011.07.019, 2011.

Pokhrel, Y., Felfelani, F., Satoh, Y., Boulange, J., Burek, P., Gädeke, A., Gerten, D., Gosling, S. N., Grillakis, M., Gudmundsson, L., Hanasaki, N., Kim, H., Koutroulis, A., Liu, J., Papadimitriou, L., Schewe, J., Müller Schmied, H., Stacke, T., Telteu, C.-E., Thiery, W., Veldkamp, T., Zhao, F., and Wada, Y.: Global terrestrial water storage and drought severity under climate change, Nat. Clim. Change, 11, 226–233, https://doi.org/10.1038/s41558-020-00972-w, 2021.

Prăvălie, R., Piticar, A., Roșca, B., Sfîcă, L., Bandoc, G., Tiscovschi, A., and Patriche, C.: Spatio-temporal changes of the climatic water balance in Romania as a response to precipitation and reference evapotranspiration trends during 1961–2013, CATENA, 172, 295–312, https://doi.org/10.1016/j.catena.2018.08.028, 2019.

Prestele, R., Alexander, P., Rounsevell, M. D. A., Arneth, A., Calvin, K., Doelman, J., Eitelberg, D. A., Engström, K., Fujimori, S., Hasegawa, T., Havlik, P., Humpenöder, F., Jain, A. K., Krisztin, T., Kyle, P., Meiyappan, P., Popp, A., Sands, R. D., Schaldach, R., Schüngel, J., Stehfest, E., Tabeau, A., Van Meijl, H., Van Vliet, J., and Verburg, P. H.: Hotspots of uncertainty in land-use and land-cover change projections: a global-scale model comparison, 22, 3967–3983, https://doi.org/10.1111/gcb.13337, 2016.

Raes, D., Steduto, P., Hsiao, T. C., and Fereres, E.: AquaCrop – the FAO crop model to simulate yield response to water: II. Main algorithms and software description, Agron. J., 101, 438–447, https://doi.org/10.2134/agronj2008.0140s, 2009.

Raes, D., Steduto, P., Hsiao, T.C., and Fereres, E. AquaCrop on-line reference manual. http://www.fao.org/nr/water/aquacrop.html, 2017.

Raes, D., Waongo, M., Vanuytrecht, E., and Mejias Moreno, P.: Improved management may alleviate some but not all of the adverse effects of climate change on crop yields in smallholder farms in West Africa, Agr. Forest Meteorol., 308–309, 108563, https://doi.org/10.1016/j.agrformet.2021.108563, 2021.

Reichle, R. H., Liu, Q., Koster, R. D., Crow, W. T., De Lannoy, G. J. M., Kimball, J. S., Ardizzone, J. V., Bosch, D., Colliander, A., Cosh, M., Kolassa, J., Mahanama, S. P., Prueger, J., Starks, P., and Walker, J. P.: Version 4 of the SMAP Level-4 Soil Moisture Algorithm and Data Product, 11, 3106–3130, https://doi.org/10.1029/2019MS001729, 2019.

Reinecke, R., Müller Schmied, H., Trautmann, T., Andersen, L. S., Burek, P., Flörke, M., Gosling, S. N., Grillakis, M., Hanasaki, N., Koutroulis, A., Pokhrel, Y., Thiery, W., Wada, Y., Yusuke, S., and Döll, P.: Uncertainty of simulated groundwater recharge at different global warming levels: a global-scale multi-model ensemble study, Hydrol. Earth Syst. Sci., 25, 787–810, https://doi.org/10.5194/hess-25-787-2021, 2021.

910 Riahi, K., Grübler, A., and Nakicenovic, N.: Scenarios of long-term socio-economic and environmental development under climate stabilization, Technol. Forecast Soc., 74, 887–935, https://doi.org/10.1016/j.techfore.2006.05.026, 2007.

Rodell, M., Houser, P. R., Jambor, U., Gottschalck, J., Mitchell, K., Meng, C.-J., Arsenault, K., Cosgrove, B., Radakovich, J., Bosilovich, M., Entin, J. K., Walker, J. P., Lohmann, D., and Toll, D.: The Global Land Data Assimilation System, B. AM. Meteorol. Soc., 85, 381–394, https://doi.org/10.1175/BAMS-85-3-381, 2004.

915 Rohwer, J., Gerten, D., and Lucht, W.: Development of functional irrigation types for improved global crop modelling, 2007.

Rosa, L., Chiarelli, D. D., Sangiorgio, M., Beltran-Peña, A. A., Rulli, M. C., D'Odorico, P., and Fung, I.: Potential for sustainable irrigation expansion in a 3 °C warmer climate, P. Natl. Acad. Sci. USA, 117, 29526–29534, https://doi.org/10.1073/pnas.2017796117, 2020.

Rosenzweig, C., Elliott, J., Deryng, D., Ruane, A. C., Müller, C., Arneth, A., Boote, K. J., Folberth, C., Glotter, M., Khabarov, 920 N., Neumann, K., Piontek, F., Pugh, T. A. M., Schmid, E., Stehfest, E., Yang, H., and Jones, J. W.: Assessing agricultural risks of climate change in the 21st century in a global gridded crop model intercomparison, P. Natl. Acad. Sci. USA, 111, 3268–3273, https://doi.org/10.1073/pnas.1222463110, 2014.

Rosenzweig, C., Arnell, N. W., Ebi, K. L., Lotze-Campen, H., Raes, F., Rapley, C., Smith, M. S., Cramer, W., Frieler, K., Reyer, C. P. O., Schewe, J., Vuuren, D. van, and Warszawski, L.: Assessing inter-sectoral climate change risks: the role of 925 ISIMIP, Environ. Res. Lett., 12, 010301, https://doi.org/10.1088/1748-9326/12/1/010301, 2017.

Ruosteenoja, K., Markkanen, T., Venäläinen, A., Räisänen, P., and Peltola, H.: Seasonal soil moisture and drought occurrence in Europe in CMIP5 projections for the 21st century, Clim. Dynam., 50, 1177–1192, https://doi.org/10.1007/s00382-017-3671-4, 2018.

Russo, S., Dosio, A., Sterl, A., Barbosa, P., and Vogt, J.: Projection of occurrence of extreme dry-wet years and seasons in 930 Europe with stationary and nonstationary Standardized Precipitation Indices, J. Geophys. Res.-Atmos, 118, 7628–7639, https://doi.org/10.1002/jgrd.50571, 2013.

Satoh, Y., Shiogama, H., Hanasaki, N., Pokhrel, Y., Boulange, J. E. S., Burek, P., Gosling, S. N., Grillakis, M., Koutroulis, A., Schmied, H. M., Thiery, W., and Yokohata, T.: A quantitative evaluation of the issue of drought definition: a source of disagreement in future drought assessments, Environ. Res. Lett., 16, 104001, https://doi.org/10.1088/1748-9326/ac2348, 2021.

935 Schaldach, R., Koch, J., Aus der Beek, T., Kynast, E., and Flörke, M.: Current and future irrigation water requirements in pan-Europe: An integrated analysis of socio-economic and climate scenarios, Global Planet. Change, 94–95, 33–45, https://doi.org/10.1016/j.gloplacha.2012.06.004, 2012.

Schleussner, C.-F., Deryng, D., Müller, C., Elliott, J., Saeed, F., Folberth, C., Liu, W., Wang, X., Pugh, T. A. M., Thiery, W., Seneviratne, S. I., and Rogelj, J.: Crop productivity changes in 1.5 °C and 2 °C worlds under climate sensitivity uncertainty, 940 Environ. Res. Lett., 13, 064007, https://doi.org/10.1088/1748-9326/aab63b, 2018.

Shangguan, W., Hengl, T., Mendes de Jesus, J., Yuan, H., and Dai, Y.: Mapping the global depth to bedrock for land surface modeling, J. Adv. Model. Earth Sy., 9, 65–88, https://doi.org/10.1002/2016MS000686, 2017.

Sheffield, J. and Wood, E. F.: Projected changes in drought occurrence under future global warming from multi-model, multi-scenario, IPCC AR4 simulations, Clim. Dynam., 31, 79–105, https://doi.org/10.1007/s00382-007-0340-z, 2008.

945 Siebert, S. and Döll, P.: Quantifying blue and green virtual water contents in global crop production as well as potential production losses without irrigation, Journal of Hydrology, 384, 198–217, https://doi.org/10.1016/j.jhydrol.2009.07.031, 2010.

Siebert, S., Henrich, V., Frenken, K., and Burke, J.: Global Map of Irrigation Areas version 5, Rheinische Friedrich-Wilhelms-University, Bonn, Germany/Food and Agriculture Organization of the United Nations, Rome, Italy, [data set], available at https://www.fao.org/aquastat/en/geospatial-information/global-maps-irrigated-areas/latest-version/, (last access: 10 February 950 2021), 2013.

Siebert, S., Kummu, M., Porkka, M., Döll, P., Ramankutty, N., and Scanlon, B. R.: A global data set of the extent of irrigated land from 1900 to 2005, Hydrol. Earth Syst. Sci., 19, 1521–1545, https://doi.org/10.5194/hess-19-1521-2015, 2015.

Smith, M.: CROPWAT: A Computer Program for Irrigation Planning and Management, FAO, 140 pp., 1992.

Spinoni, J., Vogt, J. V., Naumann, G., Barbosa, P., and Dosio, A.: Will drought events become more frequent and severe in 955 Europe?, Int. J. Climatol., 38, 1718–1736, https://doi.org/10.1002/joc.5291, 2018.

Steduto, P., Hsiao, T. C., Raes, D., and Fereres, E.: AquaCrop—The FAO Crop Model to Simulate Yield Response to Water: I. Concepts and Underlying Principles, Agron. J., 101, 426–437, https://doi.org/10.2134/agronj2008.0139s, 2009.

Stöckle, C.Still, C. J., Berry, J. A., Collatz, G. J., and DeFries, R. S.: Global distribution of C3 and C4 vegetation: Carbon cycle implications, 17, 6-1-6–14, https://doi.org/10.1029/2001GB001807, 2003.Stöckle, C. O., Kemanian, A. R., Nelson, R. 960 L., Adam, J. C., Sommer, R., and Carlson, B.: CropSyst model evolution: From field to regional to global scales and from research to decision support systems, Environ. Modell. Softw., 62, 361–369, https://doi.org/10.1016/j.envsoft.2014.09.006, 2014.

Taylor, R. G., Scanlon, B., Döll, P., Rodell, M., van Beek, R., Wada, Y., Longuevergne, L., Leblanc, M., Famiglietti, J. S., Edmunds, M., Konikow, L., Green, T. R., Chen, J., Taniguchi, M., Bierkens, M. F. P., MacDonald, A., Fan, Y., Maxwell, R. 965 M., Yechieli, Y., Gurdak, J. J., Allen, D. M., Shamsudduha, M., Hiscock, K., Yeh, P. J.-F., Holman, I., and Treidel, H.: Ground water and climate change, Nat. Clim. Change, 3, 322–329, https://doi.org/10.1038/nclimate1744, 2013.

Telteu, C.-E., Müller Schmied, H., Thiery, W., Leng, G., Burek, P., Liu, X., Boulange, J. E. S., Andersen, L. S., Grillakis, M., Gosling, S. N., Satoh, Y., Rakovec, O., Stacke, T., Chang, J., Wanders, N., Shah, H. L., Trautmann, T., Mao, G., Hanasaki, N., Koutroulis, A., Pokhrel, Y., Samaniego, L., Wada, Y., Mishra, V., Liu, J., Döll, P., Zhao, F., Gädeke, A., Rabin, S. S., and 970 Herz, F.: Understanding each other's models: an introduction and a standard representation of 16 global water models to support intercomparison, improvement, and communication, Geosci. Model Dev., 14, 3843–3878, https://doi.org/10.5194/gmd-14-3843-2021, 2021.

Thiery, W., Davin, E. L., Lawrence, D. M., Hirsch, A. L., Hauser, M., and Seneviratne, S. I.: Present-day irrigation mitigates heat extremes, J. Geophys. Res.-Atmos, 122, 1403–1422, https://doi.org/10.1002/2016JD025740, 2017.

975 Thiery, W., Visser, A. J., Fischer, E. M., Hauser, M., Hirsch, A. L., Lawrence, D. M., Lejeune, Q., Davin, E. L., and Seneviratne, S. I.: Warming of hot extremes alleviated by expanding irrigation, Nat. Commun., 11, 290, https://doi.org/10.1038/s41467-019-14075-4, 2020.

Thiery, W., Lange, S., Rogelj, J., Schleussner, C.-F., Gudmundsson, L., Seneviratne, S. I., Andrijevic, M., Frieler, K., Emanuel, K., Geiger, T., Bresch, D. N., Zhao, F., Willner, S. N., Büchner, M., Volkholz, J., Bauer, N., Chang, J., Ciais, P., Dury, M., 980 François, L., Grillakis, M., Gosling, S. N., Hanasaki, N., Hickler, T., Huber, V., Ito, A., Jägermeyr, J., Khabarov, N.,

Koutroulis, A., Liu, W., Lutz, W., Mengel, M., Müller, C., Ostberg, S., Reyer, C. P. O., Stacke, T., and Wada, Y.: Intergenerational inequities in exposure to climate extremes, Science, 374, 158–160, https://doi.org/10.1126/science.abi7339, 2021.

van Vuuren, D. P., Edmonds, J., Kainuma, M., Riahi, K., Thomson, A., Hibbard, K., Hurtt, G. C., Kram, T., Krey, V., Lamarque, J.-F., Masui, T., Meinshausen, M., Nakicenovic, N., Smith, S. J., and Rose, S. K.: The representative concentration pathways: an overview, Climatic Change, 109, 5, https://doi.org/10.1007/s10584-011-0148-z, 2011.

van Vuuren, D. P., Kriegler, E., O'Neill, B. C., Ebi, K. L., Riahi, K., Carter, T. R., Edmonds, J., Hallegatte, S., Kram, T., Mathur, R., and Winkler, H.: A new scenario framework for Climate Change Research: scenario matrix architecture, Climatic Change, 122, 373–386, https://doi.org/10.1007/s10584-013-0906-1, 2014.

Vanuytrecht, E.: The effects on crop cultivation of increased CO2, temperature and ozone levels due to climate change, Burleigh Dodds Science Publishing Ltd; Cambridge, https://doi.org/10.19103/AS.2020.0064.01, 2020.

Vanuytrecht, E., Raes, D., and Willems, P.: Considering sink strength to model crop production under elevated atmospheric CO2, Agr. Forest Meterol., 151, 1753–1762, https://doi.org/10.1016/j.agrformet.2011.07.011, 2011.

Vanuytrecht, E., Raes, D., Willems, P., and Geerts, S.: Quantifying field-scale effects of elevated carbon dioxide concentration on crops, Clim. Res., 54, 35–47, https://doi.org/10.3354/cr01096, 2012.

Vicente-Serrano, S. M., Van der Schrier, G., Beguería, S., Azorin-Molina, C., and Lopez-Moreno, J.-I.: Contribution of precipitation and reference evapotranspiration to drought indices under different climates, J. Hydrol., 526, 42–54, https://doi.org/10.1016/j.jhydrol.2014.11.025, 2015.

Wada, Y., Wisser, D., Eisner, S., Flörke, M., Gerten, D., Haddeland, I., Hanasaki, N., Masaki, Y., Portmann, F. T., Stacke, T., Tessler, Z., and Schewe, J.: Multimodel projections and uncertainties of irrigation water demand under climate change, Geophys. Res. Lett., 40, 4626–4632, https://doi.org/10.1002/grl.50686, 2013.

Warszawski, L., Frieler, K., Huber, V., Piontek, F., Serdeczny, O., and Schewe, J.: The Inter-Sectoral Impact Model Intercomparison Project (ISI–MIP): Project framework, P. Natl. Acad. Sci. USA, 111, 3228–3232, https://doi.org/10.1073/pnas.1312330110, 2014.

Webber, H., Gaiser, T., Oomen, R., Teixeira, E., Zhao, G., Wallach, D., Zimmermann, A., and Ewert, F.: Uncertainty in future irrigation water demand and risk of crop failure for maize in Europe, Environ. Res. Lett., 11, 074007, https://doi.org/10.1088/1748-9326/11/7/074007, 2016.

Williams, J. R., Jones, C. A., Kiniry, J. R., and Spanel, D. A.: The EPIC Crop Growth Model, Transactions of the ASAE, 32, 497–0511, https://doi.org/10.13031/2013.31032, 1989.

Wriedt, G., Van der Velde, M., Aloe, A., and Bouraoui, F.: Estimating irrigation water requirements in Europe, J. Hydrol., 373, 527–544, https://doi.org/10.1016/j.jhydrol.2009.05.018, 2009.